https://doi.org/10.5194/gmd-2019-212
Preprint. Discussion started: 3 September 2019

Geoscientific Model Development Discussions

A new approach to simulate aerosol effects on cirrus clouds in EMAC v2.54

Mattia Righi[1], Johannes Hendricks[1], Ulrike Lohmann[2], Christof Gerhard Beer[1], Valerian Hahn[1], Bernd Heinold[3], Romy Heller[1], Martina Krämer[4], Christian Rolf[4], Ina Tegen[3], and Christiane Voigt[1]

[1]Deutsches Zentrum für Luft- und Raumfahrt (DLR), Institut für Physik der Atmosphäre, Oberpfaffenhofen, Germany
[2]Institute for Atmospheric and Climate Science, ETH Zürich, Zürich, Switzerland
[3]Leibniz Institute for Tropospheric Research (TROPOS), Leipzig, Germany
[4]Research Centre Jülich, Institute for Energy and Climate Research 7: Stratosphere (IEK-7), Jülich, Germany

Correspondence to: Mattia Righi (mattia.righi@dlr.de)

Abstract. A new cloud microphysical scheme including a detailed parameterization for aerosol-driven ice formation in cirrus clouds is implemented in the global chemistry climate model EMAC and coupled to the aerosol submodel MADE3. The new scheme is able to consistently simulate three regimes of stratiform clouds (liquid, mixed- and ice-phase (cirrus) clouds), considering the impact of aerosol on the activation of cloud droplets and the nucleation of ice crystals. In the cirrus regime, it accounts for the competition between homogeneous and heterogeneous freezing for the available supersaturated water vapor, taking into account different types of ice-nucleating particles, whose specific ice-nucleating properties can be flexibly varied in the model setup. The new model configuration was tuned using satellite data to find the optimal set of parameters that reproduces the observations. A detailed evaluation is also performed comparing the model results for standard cloud and radiation variables with a comprehensive set of observations from satellite retrievals and in situ measurements. The performance of EMAC-MADE3 in this new coupled configuration is in line with similar global coupled models and with other global aerosol models featuring ice cloud parameterizations. Some remaining discrepancies, especially with regard to ice crystal number concentrations in cirrus, which are a common problem of this kind of models, need to be the subject of future investigations. To further demonstrate the readiness of the new model system for application studies, an estimate of the global anthropogenic aerosol radiative forcing is provided and discussed in the context of the CMIP5 results for the IPCC.

1 Introduction

The impact of aerosol on atmospheric composition and climate still represents one of the largest uncertainties in the quantification of anthropogenic climate change (Boucher et al., 2013). Aerosol particles influence the Earth's radiation budget via scattering and absorption of incoming solar radiation (aerosol-radiation interactions) or indirectly by changing cloud microphysical and radiative properties (aerosol-cloud interactions). The level of scientific understanding of the underlying processes is still relatively low and their representation in global models, which are the only available tools for estimating climate impacts, is challenging.

https://doi.org/10.5194/gmd-2019-212
Preprint. Discussion started: 3 September 2019

Geoscientific Model Development Discussions

This is particularly the case for aerosol-cloud interactions, which require a detailed knowledge of various processes acting on a wide range of spatial and temporal scales. Aerosol particles can act as cloud condensation nuclei (CCN) for the formation of cloud droplets in liquid clouds (Andreae et al., 2005; McFiggans et al., 2006). This process is controlled by the microphysical properties of the CCN (such as number concentration, size and chemical composition), but also depends on the mesoscale and large-scale atmospheric dynamics, which determine the occurrence and strength of vertical updrafts, leading in turn to cooling of the rising air parcels and supersaturation of water vapor available for condensation. In recent years, significant progress has been made in developing parameterizations for describing the aerosol activation process in liquid clouds in the framework of global models (see Ghan et al., 2011, for a review), but the uncertainties remain large.

Even more complex is the aerosol-induced formation of ice crystals. At atmospheric conditions, the direct freezing of supercooled liquid solutions requires very high relative humidity above $\mathrm{RH_{ice}} = 140\%$. This process is called homogeneous freezing and can only occur at temperatures below the so-called homogeneous freezing threshold, around 235 K (Koop et al., 2000). At lower supersaturations and higher temperatures, ice crystals form in the presence of an ice-nucleating particle (INP), which reduces the energy barrier for initiating the freezing process, thus lowering the relative humidity threshold for the formation of ice crystals. This process is collectively termed heterogeneous freezing, but it actually occurs along several formation pathways, depending on the properties of the involved INP and on the supersaturation (Vali et al., 2015): immersion freezing (initiated by an INP immersed in a cloud or solution droplet), contact freezing (initiated by the collision of a supercooled water droplet with a solid INP), condensation freezing (condensation of water vapor on the surface of an INP and subsequent, almost concurrent, freezing), and deposition nucleation (direct deposition of water vapor on the surface of an INP). Only a small subset (0.01-0.001 %) of the aerosol particles in the atmosphere can act as INPs. In situ measurements and laboratory studies showed that in particular mineral dust, black carbon, organic and biogenic particles can serve as INPs across a wide range of ice supersaturations (Hoose and Möhler, 2012; Cziczo et al., 2013; Kanji et al., 2017), but large uncertainties still exist on the freezing properties of the aerosol particles. The role of INPs is particularly complex in the cirrus regime, i.e. at temperatures below the homogeneous freezing threshold, since they lead to a competition between homogeneous and heterogeneous freezing for the available supersaturated water vapor. The dominance of either process over the other is essential in determining the number concentration and size of the formed ice crystals, affecting the properties of the cirrus cloud (Kärcher et al., 2006; Spichtinger and Gierens, 2009).

In this paper, we describe and evaluate the implementation of a new two-moment cloud microphysical scheme (Kuebbeler et al., 2014) into the global model EMAC (ECHAM/MESSy Atmospheric Chemistry; Jöckel et al., 2010) and its coupling to the aerosol microphysics submodel MADE3 (Modal Aerosol Dynamics model for Europe adapted for global applications, third generation; Kaiser et al., 2019) submodel. The new cloud scheme is based on a previous scheme by Lohmann and Hoose (2009) already available in EMAC, but it now includes the parameterization of aerosol-induced cirrus cloud formation by Kärcher et al. (2006). This parameterization describes the ice formation processes in cirrus clouds depending on the properties of the INPs, while accounting for the competition between homogeneous and heterogeneous ice formation. Whereas Kuebbeler et al. (2014) only considered heterogeneous freezing of mineral dust, in this study we further extend the parameterization to also account for black carbon (BC) as a possible INP. The ice-nucleating properties of the different types of BC are

https://doi.org/10.5194/gmd-2019-212
Preprint. Discussion started: 3 September 2019

Geoscientific Model Development Discussions

however still highly debated. Here, we assume that BC can form ice via deposition nucleation and assume a single freezing mode for BC, like Hendricks et al. (2011), although no clear experimental confirmation exists that supports this hypothesis. Recent studies, for instance, observed BC nucleation at cirrus temperatures but explained it with pore condensation and freezing rather than with deposition nucleation (Marcolli, 2017; Mahrt et al., 2018; David et al., 2019). Despite the relative lack of experimental support on the ice formation ability of BC in the cirrus regime, its role in ice cloud formation is potentially relevant and the resulting climate impacts could be significant, especially when considering specific emission sources such as aviation (Koehler et al., 2009; Hendricks et al., 2011; Zhou and Penner, 2014; Penner et al., 2018; Urbanek et al., 2018) or land transport (Kulkarni et al., 2016). One of the main application targets for this model will be the improvement of the current estimates on the climate impact of the transport sectors (Righi et al., 2013, 2015b, 2016), also considering the role of cirrus clouds, which motivates the consideration of BC as possible INP in the cirrus parameterization implemented here.

The new model configuration was tuned to obtain an optimal agreement in the representation of key cloud and radiation variables in comparison with the observational values reported in the literature. The tuned setup was then evaluated in detail against a wide range of satellite, ground-based and aircraft data. As a first example of application we simulated the global aerosol radiative forcing effect from anthropogenic emissions with respect to pre-industrial times. This estimate will serve as a basis for future application studies on specific sectors, for which the new model configuration described here is specifically designed.

There are still only few global models capable of simulating aerosol-induced ice formation in the cirrus regime in detail and of estimating the resulting climate impacts. In a recent development work, Bacer et al. (2018) coupled the Global Modal-aerosol eXtension (GMXe) submodel (Pringle et al., 2010) to the cirrus parameterization by Barahona and Nenes (2009) in the EMAC model, opening interesting perspectives for comparing different aerosol and cloud microphysical schemes within the same model framework. Penner et al. (2018) included an ice-formation parameterization for cirrus clouds in the NCAR-CAM5.3 model coupled to the IMPACT aerosol model, also distinguishing three aerosol mixing states in three size modes. Their resulting estimates of the radiative forcing from various emission sources show a potentially large impact of aerosol-induced cirrus modifications on climate, although other studies (Hendricks et al., 2011; Gettelman and Chen, 2013) found no statistically significant effects. The compelling need for additional insights into this issue motivated the extension of MADE3 towards a better resolved representation of INP properties (Kaiser et al., 2019) and the coupling to a new cloud scheme with a detailed parameterization for aerosol-induced ice formation in cirrus clouds, which is described in the present paper. Since, as discussed above, experimental support for the ice-nucleating properties of BC are still very limited, the modeling tools need to be designed in such a way that different assumptions can be flexibly and efficiently assessed by means of sensitivity studies, in order to explore the parameter space and provide a more precise uncertainty estimate for the resulting effects on climate.

The paper is organized as follows: the EMAC-MADE3 model and its configuration is described in Sect. 2. The implementation of the new cloud scheme with the cirrus parameterization is detailed in Sect. 3. Section 4 deals with the model tuning and the comparison with observations. For demonstration, an application of the new model configuration is briefly presented in Sect. 5, where the simulated anthropogenic aerosol radiative forcing is discussed and compared with the IPCC estimates. A summary of the main conclusion of this work is then given in Sect. 6.

https://doi.org/10.5194/gmd-2019-212
Preprint. Discussion started: 3 September 2019

Geoscientific Model Development Discussions

2 Model description and configuration

We use the EMAC global model with the aerosol submodel MADE3 in the same setup as described in Kaiser et al. (2019, hereafter K19), but with an explicit representation of the interactions of aerosols with clouds and radiation, which is crucial for the present paper and the planned follow-up studies. In this section, we briefly summarize the main features of EMAC-MADE3 and discuss only the main differences with respect to the uncoupled model configuration of K19.

EMAC is a numerical chemistry and climate simulation system that includes submodels describing tropospheric and middle atmospheric processes and their interaction with oceans, land and human influences (Jöckel et al., 2010). EMAC is based on the second version of the Modular Earth Submodel System (MESSy) to link multi-institutional computer codes. The core atmospheric model is the ECHAM5 (5th generation European Centre Hamburg) general circulation model (Roeckner et al., 2006). For the present study we apply EMAC (ECHAM5 version 5.3.02, MESSy version 2.54) in the T42L19 resolution, i.e., with a spherical truncation of T42 (corresponding to a quadratic Gaussian grid of $\sim 2.8^\circ$ by 2.8° in latitude and longitude) with 19 vertical hybrid σ-pressure levels up to 10 hPa. The model time step length Δt for this resolution is 30 minutes. Unless otherwise specified, the model output is stored with a temporal resolution of 11 hours, which on average allows the full coverage of the daily cycle.

Aerosols are simulated using the aerosol submodel MADE3 (Kaiser et al., 2014), considering aerosol sulfate, ammonium, nitrate, sodium, chloride, particulate organic matter, black carbon, mineral dust and aerosol water. These compounds are assumed to be distributed over 9 modes, covering three size classes (Aitken, accumulation and coarse) and three particle mixing states, namely: soluble particles, insoluble particles (i.e., particles mainly composed of insoluble components, such as mineral dust or soot) and mixed particles (soluble compounds with insoluble immersions). This detailed description of particle mixing allows an advanced representation of aerosol-induced ice formation in the troposphere via different processes, which is the main focus of the current study.

As mentioned above, we apply here the same model configuration as K19, except for the submodels controlling the coupling between aerosol, clouds and radiation in the model, which are now configured to enable such coupling. The CLOUD submodel, which deals with cloud microphysics and precipitation formation in stratiform clouds at all levels, including aerosol effects on warm and mixed-phase clouds, uses the new cloud scheme by Kuebbeler et al. (2014, hereafter K14) instead of the standard ECHAM5 scheme by Roeckner et al. (2006), and is described in detail in Sect. 3. Cloud-radiation and aerosol-radiation interactions are now explicitely simulated providing the corresponding coupling parameters to the submodels CLOUDOPT (cloud cover, cloud liquid and ice water content, cloud droplet and ice crystal effective radii) and RAD (aerosol optical thickness, asymmetry factor and single scattering albedo in the respective model layers, as calculated by the AEROPT submodel). Since the present model configuration is designed to study the radiative effects of aerosol and clouds, the concentrations of radiatively active gases other than water vapor (i.e., CO_2, CH_4, N_2O, O_3 and chlorofluorocarbons) are kept constant in RAD. Further details on these submodels as part of the radiation scheme of EMAC are provided in Dietmüller et al. (2016).

https://doi.org/10.5194/gmd-2019-212
Preprint. Discussion started: 3 September 2019

Geoscientific Model Development Discussions

The simulations performed in this work cover a time period of 10 years, from 1996 to 2005, with an additional year (1995) as spin-up. As in K19, model dynamics is nudged by relaxing wind divergence and vorticity, temperature, and the logarithm of the surface pressure towards ERA-Interim reanalyses for the same time period.

Anthropogenic and biomass burning emissions of both gases and aerosols are prescribed according to the CMIP5 inventory of Lamarque et al. (2010) for the year 2000. Volcanic emissions of sulphur dioxide and primary aerosol sulfate are taken from the AeroCom inventory (Dentener et al., 2006). Wind-driven sea-salt emissions are calculated online according to the parameterization by Guelle et al. (2001). Further details about the emission setup are given in Sect. 2.4 of K19.

In contrast to K19, where dust emissions were prescribed via an offline climatology, namely the AeroCom dust climatology for the year 2000 (Dentener et al., 2006), we now apply the online parameterization developed by Tegen et al. (2002). This parameterization calculates dust emissions from 192 internal dust size classes ranging from 0.2 to 1300 μm according to the prognostic 10-meter-wind-speed and prescribed external input fields for dust source areas, soil types and vegetation cover (see Tegen et al., 2002; Stier et al., 2005; Cheng et al., 2008; Gläser et al., 2012, for more details). Mass emission fluxes of the single size classes are then grouped in two modes, which we assign to the MADE3 insoluble accumulation and coarse modes. The corresponding number emissions are then derived assuming a log-normal size distribution, with median diameters 0.42 and 1.3 μm, and mode widths sigma 1.59 and 2.0, for the accumulation and the coarse mode, respectively, following Dentener et al. (2006). In order to get a reliable representation of dust emissions with the T42 resolution used in this work, the model has been re-tuned with respect to Gläser et al. (2012) by adjusting the wind stress threshold for dust emissions as described in Tegen et al. (2004). A value of 0.845 is chosen for this parameter, in order to match the total dust emission in the AeroCom inventory for the year 2000, i.e. ~ 1700 Tg yr^{-1}, of which about 2 (98) % are emitted in the accumulation (coarse) mode. We use this dataset as a reference since it is well evaluated and widely used in several global modeling studies (Huneeus et al., 2011). An additional correction is introduced to avoid artefacts of extremely high emissions in model grid boxes near the Himalayan region. These artefacts dominate global dust emissions and are up to 1000 times higher in the current setup than the corresponding values in the AeroCom dataset. Due to the relatively low spatial model resolution, strong dust sources in this region (namely the Taklamakan desert) coincide with high surface winds (resulting from the steep orography gradient at the northern slope of the Himalayas) within the same model grid box. This results in unrealistically high dust emissions in such grid boxes, as also noted by Gläser et al. (2012), who found that these artefacts vanish at horizontal resolutions of T85 and higher. In our setup, these artifacts are removed by setting a threshold height for the orography, above which emission fluxes are set to zero. This is set to 2500 m for the present resolution.

3 Cloud microphysical scheme and coupling to aerosol

In the present study we use a detailed cloud microphysical scheme which describes aerosol-driven formation of cloud droplets and ice crystals. An important feature of this cloud scheme is a detailed parameterization of aerosol-induced formation of ice crystals in the cirrus regime (Kärcher et al., 2006; Hendricks et al., 2011). The cloud scheme has originally been developed by K14 for the ECHAM5 model and coupled to the Hamburg Aerosol Model (HAM, Stier et al., 2005). Here we implement the

https://doi.org/10.5194/gmd-2019-212
Preprint. Discussion started: 3 September 2019

Geoscientific Model Development Discussions

cloud scheme in the MESSy framework and couple it to MADE3. With respect to HAM, MADE3 provides a more detailed description of aerosol mixing states, using 9 instead of 7 modes explicitely distinguishing between purely insoluble and mixed particles. This is especially important for the ice phase, since formation of ice crystals in the troposphere can occur along different pathways, depending on the properties of the INPs that initiate the process.

The cloud scheme solves prognostic equations for cloud liquid water content, ice content, cloud droplet and ice crystal number concentrations, considering aerosol-induced formation of cloud droplets and ice crystals, as well as rain and snow formation, condensational and depositional growth, evaporation of cloud water and rain, sublimation or melting of cloud ice and snow, freezing of cloud water, as well as sedimentation of cloud ice (Lohmann et al., 2007, 2008). Cloud cover is treated diagnostically using the Sundqvist scheme, which assumes partial cloud cover above a critical threshold of relative humidity and full coverage at saturation (Sundqvist et al., 1989). Sub-grid scale variability of the vertical velocity, i.e. vertical updrafts, which cannot be resolved by the global model due to its coarse resolution, is accounted for as in Lohmann and Kärcher (2002) by adding a turbulent component ω_t to the large-scale vertical velocity ω_{ls} proportional to square root of the turbulent kinetic energy (TKE):

$$\omega = \omega_{ls} + \omega_t + \omega_{gw} = \omega_{ls} + c\sqrt{\mathrm{TKE}} + \omega_{gw} \tag{1}$$

Here, we choose $c = 1.33$ for liquid and mixed-phase clouds (Lohmann et al., 2007) and $c = 0.7$ for cirrus (Kärcher and Lohmann, 2002). As in K14, we also consider the effect of orographic gravity waves on the vertical velocity, by adding a further term ω_{gw} to the right hand side of Eq. (1). In EMAC, this component is calculated by the submodel OROGW which implements the parameterization by Joos et al. (2008) originally developed for ECHAM5 and used in K14.

In the cloud scheme three different regimes of stratiform clouds are distinguished: liquid clouds ($T > 273.15$ K), mixed-phase clouds ($238.15 \leq T \leq 273.15$ K) and ice clouds ($T < 238.15$ K), each using dedicated microphysical parameterizations. Formation of cloud droplets is described following Abdul-Razzak and Ghan (2000), calculating the fraction of activated aerosol particles at a given supersaturation as a function of their radius and composition. Here, it is assumed that only the soluble compounds (SO_4^{2-}, NO_3^-, NH_4^+, Na^+ and Cl^-) contribute to the mean hygroscopicity parameter which controls the critical supersaturation for particle activation. An alternative formulation by Petters and Kreidenweis (2007) to calculate the supersaturation based on a single κ parameter has also been implemented in EMAC and coupled to MADE3 in this work. Results of sensitivity simulations (see Sect. 4.3), however, revealed no significant differences in cloud droplet number concentration (CDNC) obtained with the different approaches and the Abdul-Razzak and Ghan (2000) approach is used to calculate the supersaturation in the simulation evaluated in this work.

Formation of ice crystals is described using different parameterizations for mixed-phase and cirrus clouds. In the mixed-phase regime, ice formation is assumed to occur via contact nucleation of dust particles and immersion freezing of BC and dust particles, according to the description by Lohmann and Diehl (2006) and Hoose et al. (2008). Dust is assumed to behave like a montmorillonite mineral in terms of its INP properties. Deposition nucleation of BC in the mixed-phase regime is considered to be negligible and not included. The Bergeron-Findeisen process (Bergeron, 1928; Findeisen, 1938) is parameterized according to Lohmann et al. (2007).

https://doi.org/10.5194/gmd-2019-212
Preprint. Discussion started: 3 September 2019

Geoscientific Model Development Discussions

In the cirrus regime ($T < 238.15$ K), the parameterization by Kärcher et al. (2006) is used, which considers ice formation through the competition of various ice formation mechanisms for condensable water vapor: homogeneous freezing, deposition nucleation on BC and dust, and immersion freezing on dust, as well as the growth of pre-existing ice crystals. We note again that deposition nucleation of BC may in reality be pore condensation and freezing (Marcolli, 2017; Mahrt et al., 2018; David et al., 2019). With respect to the original scheme by K14, in this work we further include black carbon as a potential ice-nucleating particle for heterogeneous freezing in cirrus clouds. In each of the heterogeneous freezing modes, the ice nucleation properties are described in the cloud scheme by means of two parameters: the active fraction f_a of potential INPs that actually form ice crystals and the critical supersaturation S_c at which the freezing starts. The values assumed in this study for these parameters are summarized in Table 1: for deposition nucleation of insoluble dust and immersion freezing of coated (mixed) dust, we use the same values as K14, based on the laboratory studies by Möhler et al. (2006, 2008). For ice nucleation of BC we follow Hendricks et al. (2011).

Table 1. Ice nucleation properties assumed for the different modes of heterogeneous ice formation in the cirrus scheme: ice active fraction f_a and critical supersaturation S_c. S_i is the ice supersaturation.

Ice mode		S_c	f_a	Reference
Dust deposition	$T \leq 220$K	1.1	$\exp\left[2\left(S_i - S_c\right)\right] - 1$	Kuebbeler et al. (2014)
	$T > 220$K	1.2	$\exp\left[0.5\left(S_i - S_c\right)\right] - 1$	
Dust immersion		1.3	0.05	Kuebbeler et al. (2014)
BC		1.4	0.0025	Hendricks et al. (2011)

The number concentrations of potential INPs for the different ice formation processes must be provided as input to both the mixed-phase and the cirrus cloud parameterization. With respect to the work by K14, the calculation of these parameters has been completely revised here, to account for the structural differences between the HAM and MADE3 aerosol modules, the latter providing a more detailed description of aerosol mixing states. The details of this calculation are provided in Appendix A.

4 Model evaluation

In this section we evaluate the performance of EMAC-MADE3 in the coupled configuration. The representation of aerosol quantities such as particle mass and number concentrations, size distributions as well as aerosol optical properties has been extensively evaluated in K19 against a comprehensive pool of observational data from different sources. In K19, we concluded that MADE3 is able to capture the global pattern of aerosol mass and number distribution with deviations which are in line with the results of other aerosol global models available in the literature. The conclusions of the K19 evaluation on the aerosol representation in the uncoupled model version still hold for the coupled version discussed here, since the inclusion of cloud and radiation coupling does not lead to significant changes in the modeled global aerosol characteristics. Therefore, we focus on

https://doi.org/10.5194/gmd-2019-212
Preprint. Discussion started: 3 September 2019

Geoscientific Model Development Discussions

cloud and radiation variables in this study. We note however that this is not meant to be a detailed evaluation of the new cloud scheme adopted in this study, but rather an assessment of the overall capabilities of EMAC-MADE3 to capture the essential aspects of the aerosol-cloud and aerosol-radiation interactions.

4.1 Model tuning in comparison to observations

Following a similar approach as in Lohmann and Ferrachat (2010), we first analyze globally-averaged standard cloud and radiation variables and show how the critical tuning parameters are set in the model in order to achieve the optimal configuration. We focus in particular on the rate of rain formation by autoconversion γ_r, the rate of snow formation by aggregation γ_s, the minimum cloud droplet number concentration $\mathrm{CDNC}_{\mathrm{min}}$ and the size of newly nucleated aerosol particle d_{nuc}. The minimum CDNC is introduced in the model to avoid unrealistically low concentrations of cloud droplets in pristine conditions. The parameter d_{nuc} is used to describe the initial growth of freshly formed sulfuric-acid water clusters into larger sulfate aerosol particles. Since such nucleation and growth events frequently occur on spatial scales which cannot be resolved by the global model, the use of this parameter enables the implicit consideration of these subgrid-scale processes. In K19 a value $d_{\mathrm{nuc}} = 10$ nm was chosen, motivated by a better agreement of simulated number concentrations with observations and supported by new particle formation measurements. Here we explore how this parameter can also affect cloud and radiation variables. Lohmann and Ferrachat (2010) further considered the inhomogeneity factor of ice clouds and the entrainment rate for deep convection as tuning parameters, which in our configuration are set to 0.85 and 10^{-4} kg m^{-3} s^{-1}, respectively, but their variation is not further explored.

We tested 5 values for each of the 4 tuning parameters γ_r, γ_s, $\mathrm{CDNC}_{\mathrm{min}}$ and d_{nuc}, varying across a range of approximately one order of magnitude and calculate their effect on seven globally-averaged cloud and radiation variables in the model: liquid water path (LWP, over the oceans), ice water path (IWP), cloud droplet and ice crystal number concentrations (CDNC and ICNC), top-of-the atmosphere shortwave and longwave cloud radiative effects (SWCRE and LWCRE, as the difference between all-sky and clear-sky radiation fields), and the net radiation balance. The results are summarized and compared in Fig. 1 with global satellite data collected by Lohmann et al. (2007), Gettelman et al. (2010) and Lohmann and Neubauer (2018). When varying one of the parameters, the others are kept fixed at the reference value indicated by the red circles in the figure. A higher autoconversion rate (first column of Fig. 1) results in a more efficient removal of liquid water from the clouds via precipitation and has therefore a strong impact on LWP, which shows a variation of a factor of about 2 over the investigated range of γ_r, also impacting SWCRE and the radiation balance. To obtain the optimal agreement with all considered observations, we choose a value $\gamma_r = 8$. For the same reasons, the choice of the aggregation rate γ_s affects IWP (second column of Fig. 1), but the variation is somewhat stronger. Since the modeled IWP is too low in comparison with the observations for any choice of this parameter, we set $\gamma_s = 800$ to get a reasonable agreement with LWCRE data. The minimum CDNC (third column of Fig. 1) also indirectly controls LWP , since CDNC has a direct influence on cloud droplet size and therefore precipitation efficiency and cloud lifetime. In ECHAM-HAM, this parameters was varied between 10 and 40 cm^{-3} (Lohmann and Ferrachat, 2010, see also K14). Here we choose $\mathrm{CDNC}_{\mathrm{min}}$ =10 cm^{-3}. A better agreement with SWCRE observations could be obtained with even lower values of $\mathrm{CDNC}_{\mathrm{min}}$, but these are hardly supported by CDNC measurements, since even in pristine marine

https://doi.org/10.5194/gmd-2019-212
Preprint. Discussion started: 3 September 2019

Geoscientific Model Development Discussions

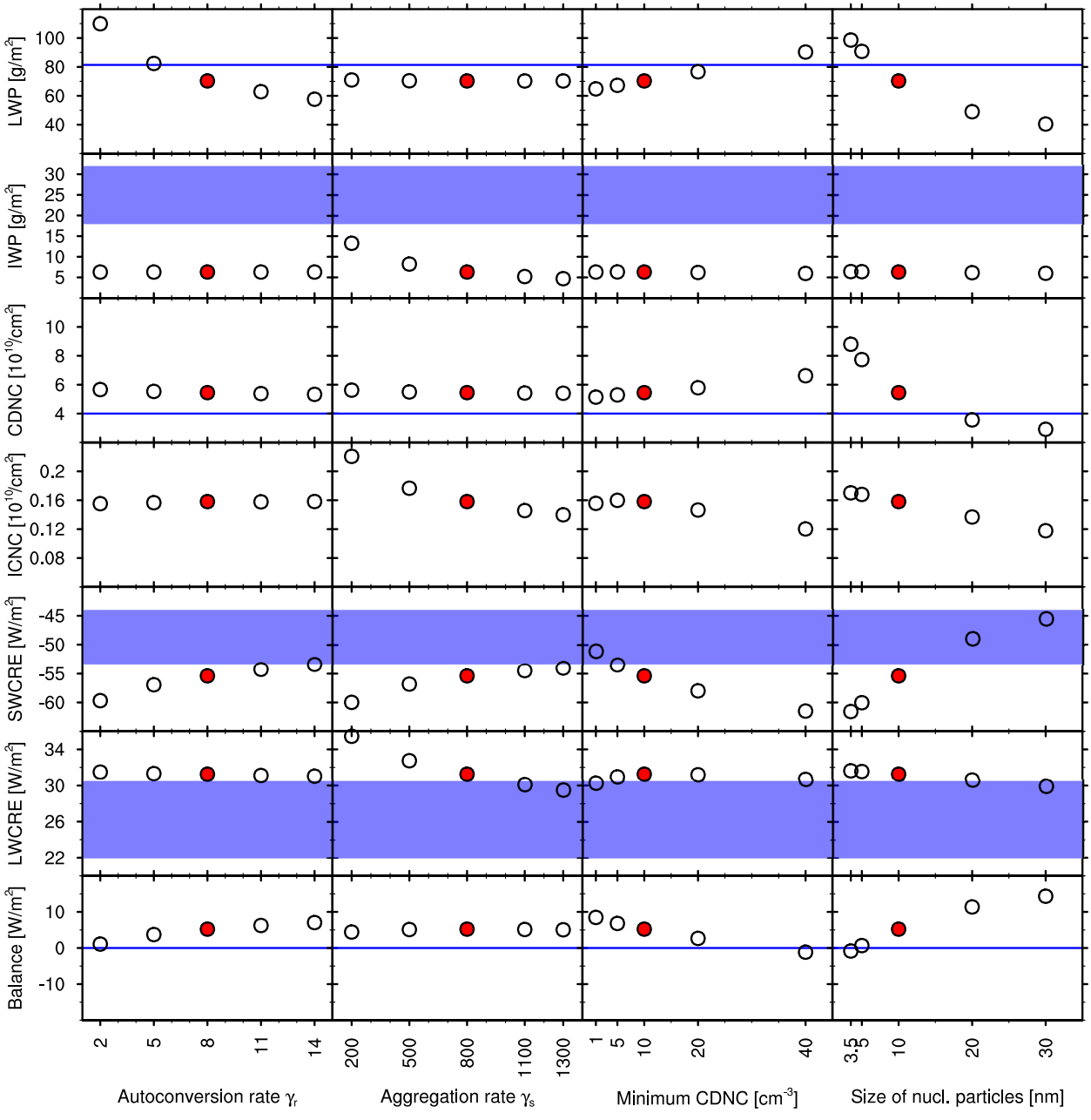

Figure 1. Results of the tuning experiments. Each column represents a tuning parameter and shows the five simulations (dots) performed with different values. Resulting values for the globally averaged cloud and radiation variables are given in each row. The red circle represents the optimal tuning configuration used for the reference simulation evaluated in this paper. The blue lines and shadings represent the observed values from a collection of satellite data given in Lohmann et al. (2007), Gettelman et al. (2010) and Lohmann and Neubauer (2018).

https://doi.org/10.5194/gmd-2019-212
Preprint. Discussion started: 3 September 2019

Geoscientific Model Development Discussions

regions CDNC around 10 cm^{-3} or more are observed (Bennartz, 2007; Karydis et al., 2011; Bennartz and Rausch, 2017). The size of newly nucleated particles has a significant impact on aerosol number concentrations, as shown by K19. Since aerosol particles serve as condensation nuclei for cloud droplet formation, this parameter primarily controls CDNC in the model also influencing LWP and SWCRE. The value d_{nuc} =10 nm, chosen by K19 motivated by the good agreement with aerosol number concentration measurements, fits well also in this context, resulting in a good agreement for the cloud variables (CDNC, LWP and SWCRE; fourth column of Fig. 1).

With the above choice of the four parameters, the model is tuned to provide a good agreement with the observed values of the main cloud variables. Table 2 summarizes the results of the tuned simulation, compared with similar experiments performed with ECHAM5-HAM by K14, ECHAM6-HAM2 by Lohmann and Neubauer (2018), EMAC-GMXe by Bacer et al. (2018) and NCAR-CAM5.3 by Penner et al. (2018). The performance of the EMAC-MADE3 coupled configuration is in line with these models and mostly within or close to the observed values given in the last column of Table 2. A notable exception is IWP, which is considerably lower than the observations and could not be improved even if using extreme values for the tuning parameters (see Fig. 1). This discrepancy could largely be due to the neglection of snow and convective ice in the IWP calculation of our model, since these ice types could give an important contributing to total ice (Waliser et al., 2009). Another reason could be the misrepresentation of the mixed-phase. To analyze the causes of this discrepancy in more detail, an advanced comparison of model IWP with satellite data, also including a set of sensitivity simulations with varying process representations, is intended to be the subject of follow-up studies. As also noted in Waliser et al. (2009), comparing cloud ice and related quantities with satellite data is however a non-trivial task, due to the difficulties in retrieving ice water content with passive instruments. We also emphasize that this model configuration has been especially developed for studies of aerosol effects on cirrus clouds and that the cirrus ice water content is simulated remarkably well by the model, as it will be shown in Sect. 4.4.

In the remaining part of this section, we complement the analysis by further evaluating the mean state of cloud and radiation variables against satellite data using the diagnostics included in the ESMValTool v1.1.0 (Eyring et al., 2016). CDNC is also compared to in situ data. Since, as mentioned above, comparing cloud ice and related quantities with satellite data is a more complex issue, which requires some caution in the interpretation of the data, we take advantage of in situ measurements from aircraft-based field campaigns to analyze ice cloud properties in cirrus clouds, which are the main focus of the present study, also in view of future applications.

4.2 Total cloud cover and cloud liquid water

In the top row of Fig. 2, multi-year average total cloud cover over the simulated time period (1996-2005) is compared with the ESA Climate Change Initiative (ESACCI) CLOUD satellite product, which is based on data from the passive imager sensors AVHRR, MODIS, ATSR-2, AATSR and MERIS (Stengel et al., 2017). The overall pattern is very well reproduced by EMAC, with a small positive bias in the tropics and a negative bias in the stratocumulus regions off the coasts of South America and Africa. These features are quite common in many global models, e.g. those participating in the CMIP3 and CMIP5 intercomparisons (Lauer and Hamilton, 2013). Larger deviations between EMAC and the observations are found in the polar regions, where, however, observational uncertainties are also larger (Lauer et al., 2017). Note that total cloud cover is only

https://doi.org/10.5194/gmd-2019-212
Preprint. Discussion started: 3 September 2019

Geoscientific Model Development Discussions
Open Access
EGU

Table 2. Summary of the globally-averaged cloud and radiation variables obtained with the reference set of tuning parameters ($\gamma_r = 8$, $\gamma_s = 800$, CDNC$_{\min}$=10 cm^{-3}, and $d_{\rm nuc} = 10$ nm) and compared with a collection of satellite observations given in Lohmann et al. (2007), Gettelman et al. (2010) and Lohmann and Neubauer (2018), and with the results of other global models: ECHAM5-HAM (Kuebbeler et al., 2014), ECHAM6-HAM2 (Lohmann and Neubauer, 2018), EMAC-GMXe (Bacer et al., 2018) and NCAR-CAM5.3 (Penner et al., 2018). All values, except effective radii, are grid means.

	This study	ECHAM5-HAM	ECHAM6-HAM2	EMAC-GMXe	NCAR-CAM5.3	Observations
LWP oceans [g/m^2]	70.3	55.6	70.6	[72.7; 76.6]	[45.7; 57.7]	81.4
IWP [g/m^2]	6.3	5.1	14.8	[11.9; 12.8]	[13.4; 20.4]	25±7
CDNC [10^{10}/m^2]	5.4	2.61	3.1	[4.12; 4.21]	[1.39; 1.77]	4.01
ICNC [10^{10}/m^2]	0.16	0.2	0.079	[0.20; 0.23]	[0.09; 0.13]	–
$r_{\rm eff}$ droplets [μm]	7.7	–	–	–	–	11.4
$r_{\rm eff}$ crystals [μm]	41.5	14.5	–	–	–	–
Water vapor [kg/m^2]	25.7	–	–	–	–	25.1
Cloud cover [%]	67.8	62.3	68.1	[69.0; 70.0]	69.3; 72.2]	68±5
Precipitation [mm/d]	2.94	2.87	2.99	[2.89; 3.03]	[2.73; 2.80]	2.7±0.2
SWCRE [W/m^2]	–55.4	–54.8	–49.9	[–58.1; –54.8]	[–66.3; –58.5]	[–53.3; –44]
LWCRE [W/m^2]	31.3	28.8	24.1	[28.9; 34.4]	[32.1; 36.7]	[22; 30.5]
Rad. balance [W/m^2]	5.23	–0.6	–	[1.53; 4.65]	–	–

weakly controlled by the specific coupling evaluated here and is rather a general feature of the core model, as demonstrated by the similar biases found by other studies using ECHAM5 and the Sundqvist et al. (1989) cloud cover scheme, such as Lohmann et al. (2007) and K14.

In the second row of Fig. 2, an analogous comparison is shown for LWP over the oceans against MAC data (Multisensor Advanced Climatology, Elsaesser et al., 2017). Although the general pattern of LWP is reproduced by EMAC, several features are not consistent with observations: in particular, EMAC tends to simulate a higher LWP in the northern extra tropics, with significantly high values in the Western Pacific, and a lower LWP in the tropics, while it agrees well with the observations in the southern extra tropics. Particularly striking is the high bias in the Northwest Pacific ocean, which may be related to a high bias in the cloud lifetime in this region. As it will be shown in the next section, CDNC is also biased high in this region in comparison to satellite data, which could in turn be the effect of a too high concentration of cloud condensation nuclei. These biases could also be partly related to the tendency of EMAC to underestimate low cloud fraction in the tropics and overestimate it in the extra-tropics (Räisänen and Järvinen, 2010; Righi et al., 2015a). As for the total cloud cover, similar deviations were found by Lauer and Hamilton (2013) in the CMIP5 multi-model mean, which is characterized by large biases in the same regions. Since the EMAC-MADE3 configuration discussed here and the CMIP5 model ensemble use the same emission inventories for anthropogenic and biomass burning sources (Lamarque et al., 2010, see also Sect. 2), uncertainties in the prescribed emission fluxes could also contribute to these biases, especially in East Asia, where anthropogenic emissions in the year 2000 are higher than in other regions of the world and have further increased since then.

https://doi.org/10.5194/gmd-2019-212
Preprint. Discussion started: 3 September 2019

Geoscientific Model Development Discussions
Open Access
EGU

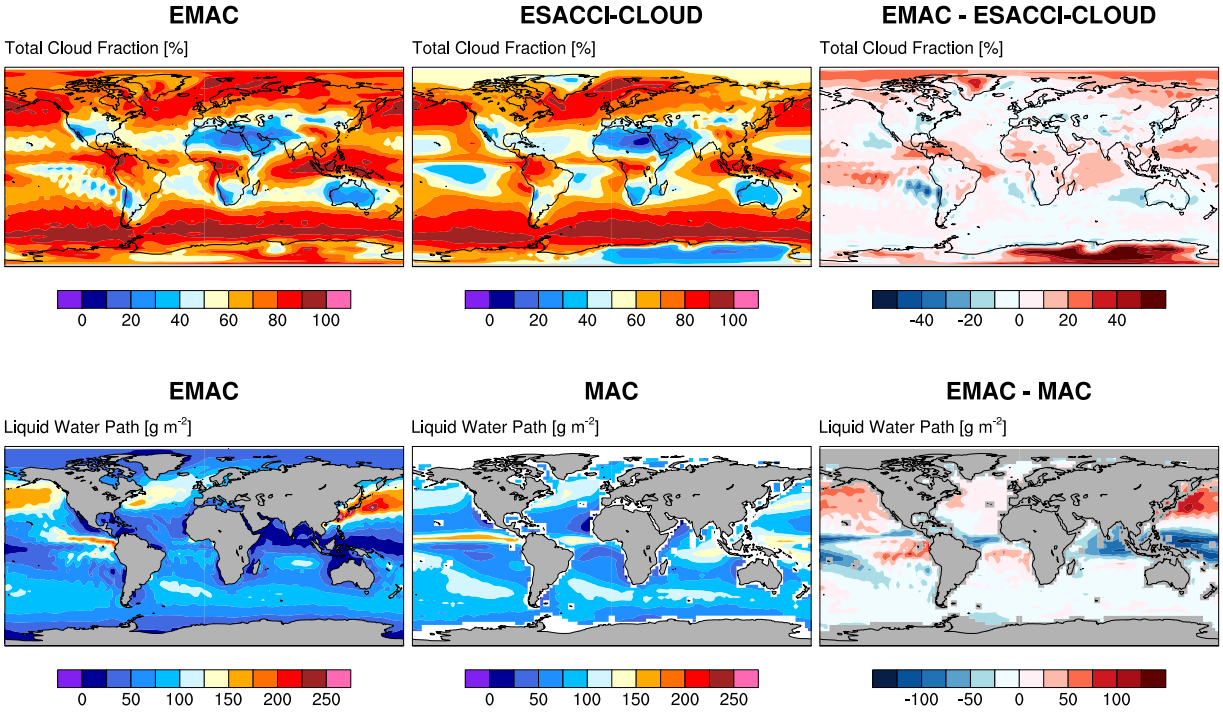

Figure 2. Multi-year (1996-2005) average total cloud cover (top row) and liquid water path (bottom row) simulated by EMAC (left), in the satellite data (middle), and the difference between model and observations (right).

4.3 Cloud droplet number concentration

We evaluate CDNC using a compilation of in situ measurements provided by Karydis et al. (2011, 2017), integrated with the measurements performed during 12 research flights during the DACCIWA campaign (Dynamics-Aerosol-Chemistry-Cloud Interactions in West Africa; Flamant et al., 2018; Taylor et al., 2019) in summer 2016 around Lomé (Togo). For this comparison, the model data are spatially colocated with the observations using a nearest-neighbor selection method for both the horizontal and the vertical coordinates. In the vertical, this is realized using the information provided for each location: either altitude (geopotential height in the model), pressure level, surface level (the lowermost hybrid model layer), or selecting the levels within the boundary-layer as calculated by the model. The time selection is performed in a climatological way, by sampling the model output at a 5-hour frequency for the same month(s) or season(s) as reported by each measurement, and averaging the selected time-steps over the whole (10 years) simulation period. For comparison with the DACCIWA data, the model output is further filtered, by selecting only the cloud scenes with a liquid water content above 0.01 $\mathrm{g\,m^{-3}}$, which is the same criterion adopted in the measurements. Reported concentrations correspond to in-cloud values.

The results of the comparison are depicted as a scatterplot in Fig. 3: considering the observational uncertainties, EMAC simulates CDNC within a factor of two (i.e., factors in the range from 0.5 to 2) of the observations in most of the regions, but

https://doi.org/10.5194/gmd-2019-212
Preprint. Discussion started: 3 September 2019

Geoscientific Model Development
Discussions
Open Access
EGU

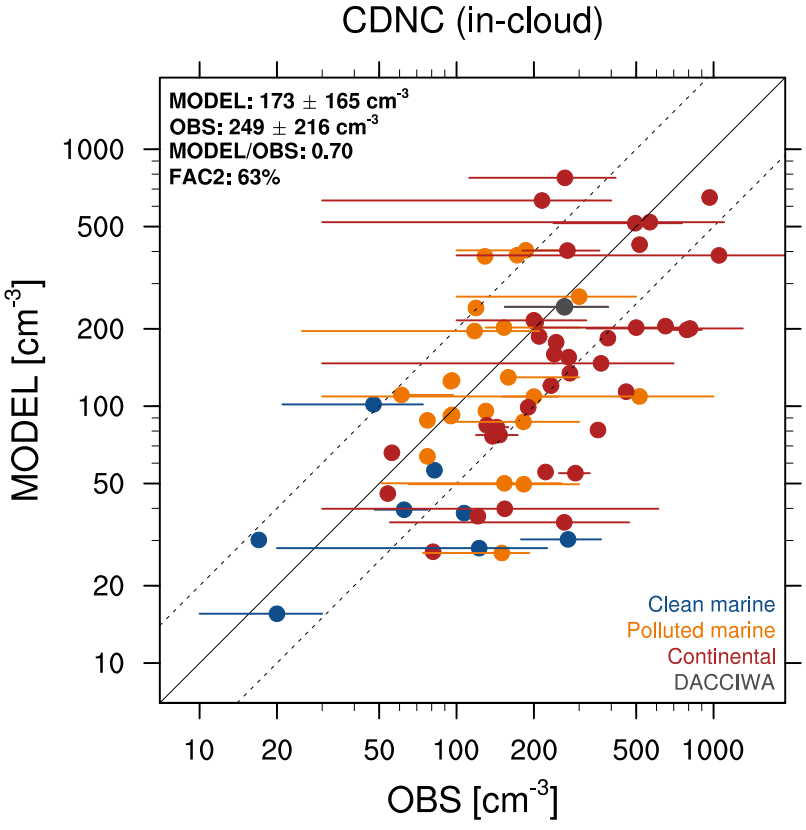

Figure 3. Scatterplot of simulated (vertical) vs. observed (horizontal) CDNC based on various satellite and in situ measurements collected by Karydis et al. (2011, 2017). Different colors represent different groups of measurement locations: clean marine (blue), polluted marine (orange) and continental (red). A further comparison with the mean of 12 flights performed during the DACCIWA campaign (Flamant et al., 2018) is shown in gray. The bars represent the range of reported values, while for the DACCIWA campaign it spans the range of the means from all flights. The mean and standard deviation of model and observations is shown on the top-left, together with their ratio and the percentage of points within a factor of 2 of the observations (FAC2, i.e. factors between 0.5 and 2).

https://doi.org/10.5194/gmd-2019-212
Preprint. Discussion started: 3 September 2019

Geoscientific Model Development Discussions

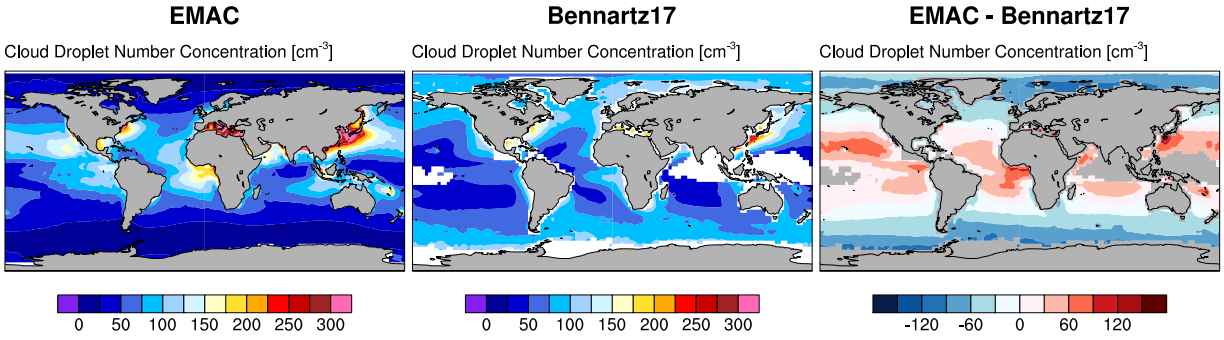

Figure 4. Similar to Fig. 2 but for CDNC at cloud top. Satellite data are averaged over the 2003-2015 time period.

it generally tends to underestimate this quantity. This is in line with recent results by Rothenberg et al. (2018), who used the MARC global aerosol model and applied various cloud droplet activation schemes. Their global integrated CDNC in the range 60–91 cm^{-3} is lower than the value simulated by EMAC (173 cm^{-3}), which is closer to the range 75–135 cm^{-3} reported by Penner et al. (2006) for three models also using the Abdul-Razzak and Ghan (2000) parameterization for cloud droplet activation.

CDNC is further compared to satellite retrievals which provide a unique global picture of this quantity. Here we use a recent 13-year climatology by Bennartz and Rausch (2017), based on MODIS-AQUA observations. In-cloud CDNC, as reported in the observational dataset, are selected with the same method used for comparing with in situ data, but considering CDNC at cloud top, as observed by the satellite, i.e. by taking the CDNC in the highest model level with a liquid cloud. An alternative method, taking the average CDNC through the cloudy part of the column, provides very similar results (not shown). This is expected, since the representation of liquid cloud formation in the EMAC cloud scheme follows the adiabatic parcel theory, assuming therefore that newly formed cloud droplets at the cloud base are equally distributed in the vertical by mixing, regardless of the aerosol concentrations. An identical assumption is also done in the retrieval process by Bennartz and Rausch (2017). The results of this comparison are depicted in Fig. 4: in the Northern Hemisphere, EMAC captures the major spots of high CDNC over the Atlantic Ocean eastward of Canada and USA, over the Mediterranean and eastward of China, albeit with about 50% higher CDNC than MODIS. These spots also have a wider horizontal extent over the oceans than in the observations. This could be due to the generally high CDNC over the continents (as shown by the in situ data in Fig. 3) being too efficiently advected over the oceans or, as mentioned in Sect. 4.2, to a bias in the prescribed emissions, causing a too high aerosol concentration and therefore a too high number of cloud condensation nuclei being activated. Another major bias is found at the Equator westward of central Africa, which could be due to biomass burning aerosol being transported over the Atlantic. Here again uncertainties in emissions of aerosols and precursor species could play a role in explaining such bias. In addition to deficiencies in the aerosol representation, the model dynamics could also explain the deviations from the observations, as for example ECHAM5 tends to be biased high in relative humidity over the tropics. Another source of uncertainty is related to the

https://doi.org/10.5194/gmd-2019-212
Preprint. Discussion started: 3 September 2019

Geoscientific Model Development Discussions
Open Access
EGU

retrieval errors in the MODIS products for effective radius and optical depth, which are used to derive CDNC. According to Bennartz and Rausch (2017), this uncertainty is around 40–50% for this datasets, with little geographical variability.

The current version of EMAC-MADE3 also allows to calculate the supersaturation in liquid clouds based on the κ-Köhler theory (Petters and Kreidenweis, 2007) as an alternative to the fitting function by Abdul-Razzak and Ghan (2000). An additional sensitivity experiment performed with this alternative formulation reveals no significant differences in the resulting CDNC (see Figures S1 and S2 in the Supplement).

4.4 Ice cloud properties

As mentioned in Sect. 4.1, evaluating the microphysical properties of ice clouds by means of satellite data is a challenging task, due to the large uncertainties of satellite retrievals of such properties (Waliser et al., 2009). Therefore, we use here a collection of in situ measurements from 18 aircraft-based field campaigns compiled into a climatology by Krämer et al. (2009) and further complemented with more recent data (see Krämer et al., 2016, Krämer et al., in prep.; a description of the respective instruments is given in these publications). The campaigns took place in several locations including Europe, Australia, Africa, Seychelles, Brazil, USA, Costa Rica, and the tropical Pacific, i.e. in the latitude band between 75° N and 25° S, for a total of 113 flights. The measurements were performed in the cirrus regime between 185 and 243 K and include several cirrus properties such as ice water content (IWC, 127.5 h of measurements), number concentration of ice crystals (ICNC, 70.9 h), ice crystal radius (R_{ice}, 65.9 hours), as well as in-cloud and clear-sky relative humidity with respect to ice (RH_{ice}, 80.9 h and 157.8 h, respectively). Consistently with the measurements, in the model only the number concentration of ice crystals in the range 3–960 μm in terms of mean volume diameter has been considered, where the mean volume diameter is defined as in Eq. (6) of Lohmann et al. (2007).

The observational data is provided as probability distribution functions in bins of 1 K in the temperature range 181 to 243 K. Cloud variables in the model (IWC, ICNC, R_{ice} and RH_{ice}) are sampled in the same range, considering only pressure levels with $p > 100$ hPa and selecting only the model grid boxes corresponding to the locations of the measurements used to generate the observational climatology. Following the same approach as K14, RH_{ice} is calculated by the cloud parameterization from air pressure p, air temperature T, specific humidity q, and saturation specific humidity with respect to ice (q_{ice}) at each model time-step:

$$RH_{ice} = 100\frac{q}{q_{ice}}, \tag{2}$$

with

$$q_{ice} = \frac{0.622\, p_{ice}}{p - 0.378\, p_{ice}} \tag{3}$$

where p_{ice} is the temperature-dependent saturation vapor pressure over ice, calculated according to Murphy and Koop (2005). To distinguish between in-cloud and cloud-free grid-boxes when comparing with the observations, the criterion IWC>0.5 mg kg^{-1} is adopted.

The results of this comparison are shown in Fig. 5 for five variables. IWC simulated by the model is in remarkably good agreement with the observations across the whole temperature range reported in the data. The observations are, however,

https://doi.org/10.5194/gmd-2019-212
Preprint. Discussion started: 3 September 2019

Geoscientific Model Development Discussions

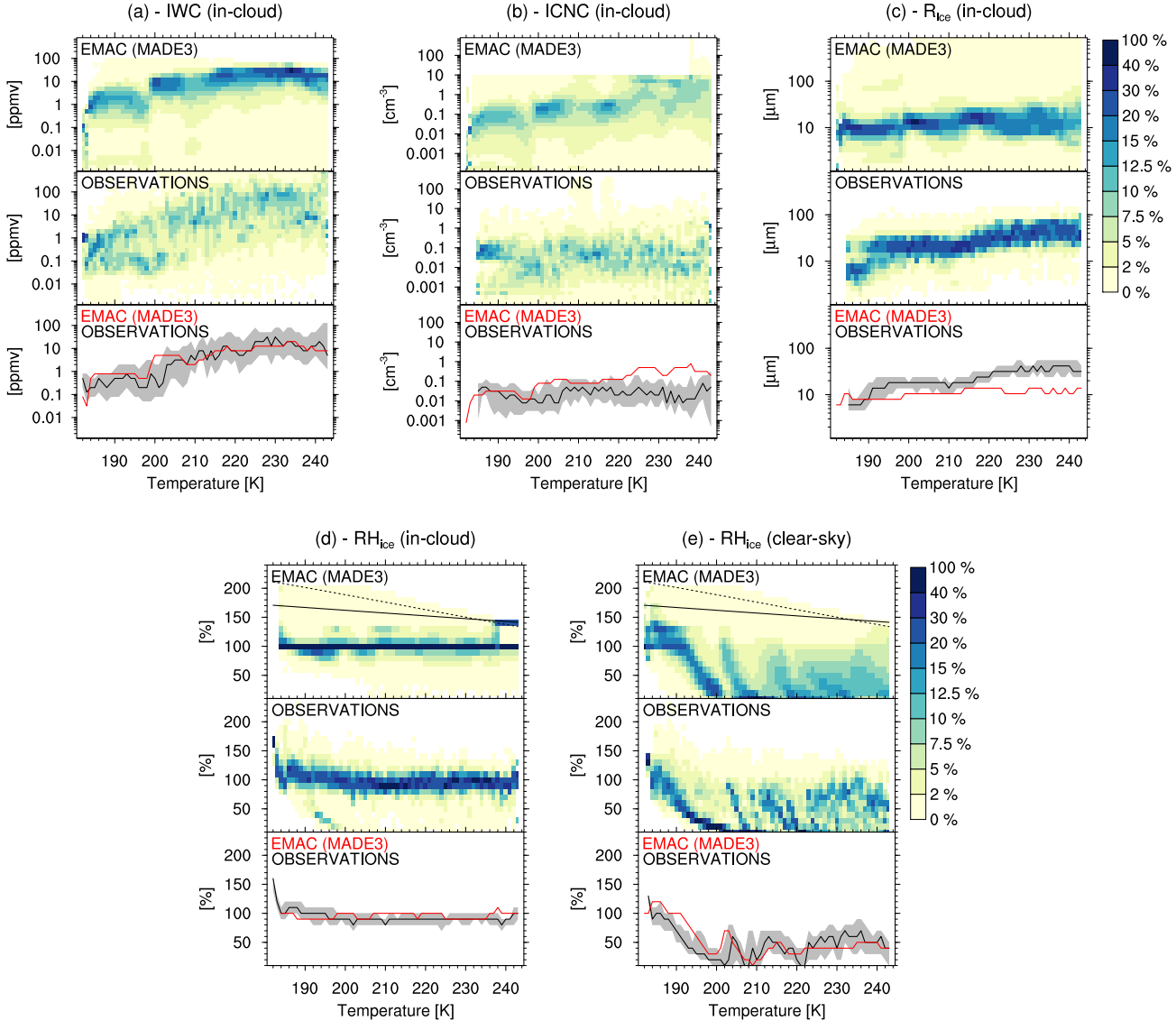

Figure 5. Climatology of various cirrus properties derived from flight campaigns as compared with EMAC (MADE3) simulations: in-cloud ice water content (a), in-cloud ice crystal number concentration (b), ice crystal mean-volume radius (c), in-cloud (d) and clear-sky (e) relative humidity with respect to ice. The data are plotted as probability distribution functions in 1-K temperature bins in the model (top plot in each panel) and in the observations (middle plot). The bottom plots in each panel show the model median (red) compared with the median (black solid line) and the 25/75% quantiles (gray shading) of the observations. The dashed and solid lines on the relative humidity panels (d, e) represent the water saturation and the homogeneous freezing threshold (Koop et al., 2000), respectively.

https://doi.org/10.5194/gmd-2019-212
Preprint. Discussion started: 3 September 2019

Geoscientific Model Development Discussions
Open Access
EGU

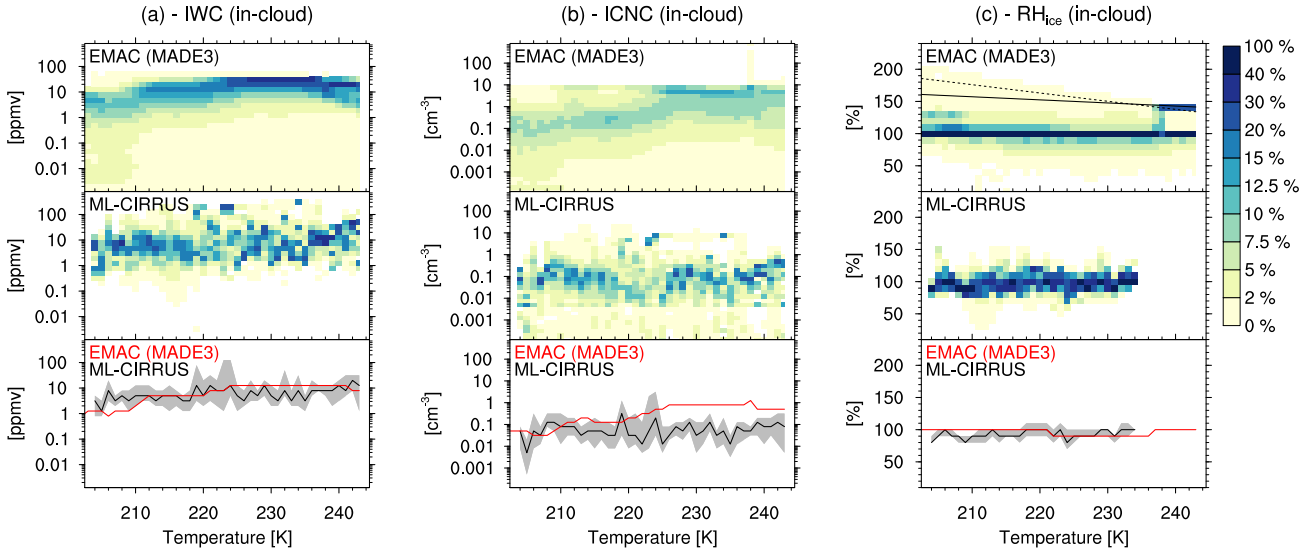

Figure 6. As in Fig. 5, but comparing to observational data from the ML-CIRRUS campaign. Shown are in-cloud ice water content (a), in-cloud ice crystal number concentration (b), in-cloud relative humidity with respect to ice (c).

characterized by a larger spread in the distribution of the IWC values in each temperature bin: this is not surprising, since the model cannot capture the small-scale variability due to its coarse resolution. The median value is nonetheless in excellent agreement with the observations, with a normalized mean bias (NMB[1]) of -11%. A good agreement is also found for ICNC, at temperatures below 215 K, while for higher temperatures significant deviations are present, and the NMB of the medians is 592%. A consistent bias is found for the mean-volume radius of the ice crystals, which is systematically lower than in the measurements ($\mathrm{NMB} = -54\%$). Relative humidity with respect to ice is very well captured by the model, both in the cloudy ($\mathrm{NMB} = 4\%$) and cloud-free ($\mathrm{NMB} = 8\%$) areas: however this is a feature which is largely controlled by the model dynamics (temperature and pressure) and is therefore only indirectly related to the aerosol-cloud coupling which is evaluated in this study.

These findings are further supported by a similar comparison to recent in-situ cirrus measurements performed during the cirrus campaign in mid-latitudes ML-CIRRUS (Voigt et al., 2017). Data from this campaign is also included in the cirrus climatology shown in Fig. 5 and discussed above (see also Krämer et al., 2016), but stem from a different set of instruments. The ML-CIRRUS climatology is based on more than 18 h of in-situ cloud observations from 13 research flights in mid-latitude cirrus clouds over Europe and the Northern Atlantic. The ice crystal number concentration is determined from three cloud probes mounted on the wings of the aircraft: the Cloud and Aerosol Spectrometer with detector for polarization CAS-DPOL (Kleine et al., 2018), the Cloud Imaging Probe CIP and the Precipitation Imaging Probe PIP (de Reus et al., 2009; Weigel et al., 2016). These three instruments cover the ice crystal size range between 3 and 6400 μm. IWC is calculated from

[1]The normalized mean bias is calculated as $\mathrm{NMB} = 100 \sum_i (M_i - O_i) / \sum_i O_i$, where M_i and O_i are the model and observation medians in each temperature bin, respectively.

https://doi.org/10.5194/gmd-2019-212
Preprint. Discussion started: 3 September 2019

Geoscientific Model Development Discussions

enhancement corrected total water measurements with the Water Vapor Analyzer (Voigt et al., 2014; Afchine et al., 2018) gas phase observations as described by Kaufmann et al. (2018). Relative humidity with respect to ice is determined from gas phase water vapor measurements of the Airborne Mass Spectrometer AIMS (Kaufmann et al., 2016). As for the global climatology, the ML-CIRRUS data for IWC, ICNC and RH_{ice} are processed in 1 K bins, but for temperatures between 203 and 243 K, as observed in mid-latitudes. To account for different spatial resolutions of the cloud particle probes, measured ICNC are averaged with a running mean of 5 seconds. The model output is processed and compared using the same method as for the global climatology, but considering only spring months (March to May) over the simulation period. The results of this comparison are shown in Fig. 6: the agreement of simulated IWC and RH_{ice} with ML-CIRRUS data is very good ($\mathrm{NMB} = 19\%$ and 3%, respectively), supporting the results from the global climatology. Also the high bias in modeled ICNC at temperatures above 225 K is confirmed for the meteorological conditions in mid-latitude cirrus, although it is slightly lower ($\mathrm{NMB} = 508\%$) than in the global climatology. We further note that the ICNC measured by ML-CIRRUS is about a factor of two higher than in the global climatology: in the temperature range 203–243 K, the average of ICNC median values in ML-CIRRUS is $0.07\,\mathrm{cm}^{-3}$, while is $0.03\,\mathrm{cm}^{-3}$ in the global climatology. This difference is also found in the model simulations, albeit with higher values due to the aforementioned bias (0.41 versus $0.26\,\mathrm{cm}^{-3}$). This is an interesting difference, which could be due to the specific meteorological and dynamic conditions encountered during the ML-CIRRUS campaign with respect to the global climatology, and their seasonality, but might also be a signature of an aircraft-induced increase in ICNC above continental Europe and in the Northern Atlantic flight corridor (see also Urbanek et al., 2018). This will be further investigated in a follow-up study on aviation impacts on cirrus clouds.

An evaluation against the same data from the Krämer et al. (2009, 2016) climatology has also been performed by Bacer et al. (2018) for two different cirrus parameterizations implemented in the EMAC-GMXe global model. For temperatures above ~ 225 K, the ICNC simulated by these two parameterizations is characterized by a high bias of about the same magnitude as the one found here. Biases are also found at lower temperatures, but they depend on the chosen parameterization. The same aircraft data has also been used by Penner et al. (2018) to evaluate ICNC in the NCAR-CAM5.3, who found a significantly high bias around 200 K, relatively independent of the assumptions on the INPs properties in their model.

4.5 Precipitation

The pattern of precipitation (Fig. 7) is reproduced remarkably well by the model compared to the data from GPCP-SG (Global Precipitation Climatology Project - Satellite and Gauge data; Adler et al., 2003). EMAC is, however, characterized by a high bias in the tropics, especially over the Pacific and Indian oceans, and small negative bias in the extra tropics; this is consistent with the biases found for liquid water path in Sect. 4.2, which anti-correlate with the precipitation biases, as expected. Interestingly, a very similar pattern of biases was found by Lamarque et al. (2013) for the models participating in ACCMIP (Atmospheric Chemistry Climate Model Intercomparison Project). These models also used the same emission inventories applied in the present study. This points again to uncertainties in the prescribed emissions as one of the possible reasons for the model deficiencies in reproducing the observations.

https://doi.org/10.5194/gmd-2019-212
Preprint. Discussion started: 3 September 2019

Geoscientific Model Development Discussions

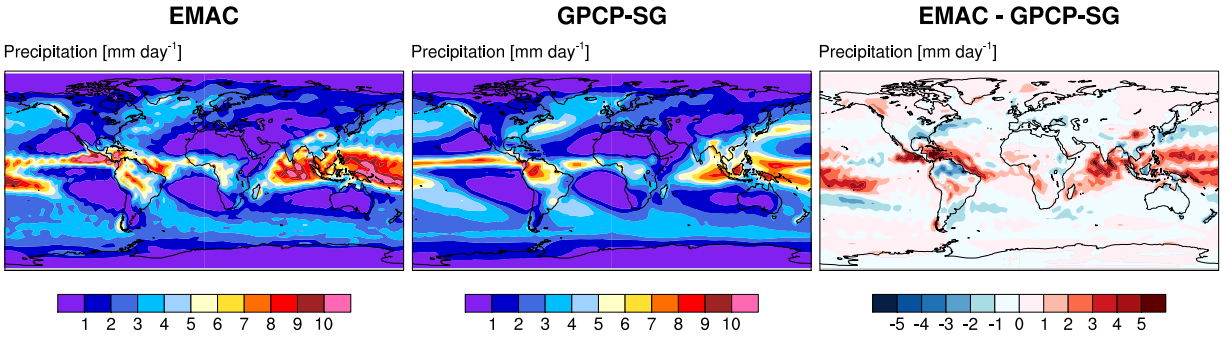

Figure 7. Similar to Fig. 2 but for precipitation.

4.6 Radiation

Figure 8 shows a similar comparison for radiation variables, namely shortwave (first row) and longwave (second row) cloud radiative effect compared to the CERES-EBAF satellite data. In the model, these quantities are given by the difference between the top-of-the-atmosphere all-sky and clear-sky fluxes, the latter being calculated via a second call to the radiation module which ignores the cloud effects (see Dietmüller et al., 2016, for details). Although the general pattern is well captured by EMAC, the shortwave cloud radiative effect is mostly overestimated over the tropics and underestimated at mid-latitudes, a picture which is consistent with the aforementioned ECHAM5 bias in low cloud cover (Räisänen and Järvinen, 2010). As noted by Räisänen and Järvinen, this is relatively independent of the cloud fraction scheme and can be ascribed to other model components, such as the convection scheme and the boundary-layer scheme (see also Righi et al., 2015a). It is therefore not related to the specific model configuration which is being evaluated in this work. Longwave cloud radiative effect is also reasonably well represented in the model, although with a generally positive bias, which is strong over Central America and the Indian Ocean.

5 Anthropogenic aerosol RF effect

As a further characterization of model performance, we calculate the anthropogenic aerosol radiative forcing using the new model configuration. We quantify this as the difference in the top-of-the-atmosphere all-sky shortwave and longwave fluxes between the reference simulation and a similar experiment, where the 1850 (pre-industrial) emissions for anthropogenic and biomass burning sources are used instead of the 2000 (present day) ones. Other emissions, such as those from natural sources, are left unchanged between the two experiments. As mentioned in Sect. 2, radiatively active gases are kept constant, so that the resulting radiative forcing is solely due to changes in the concentrations of aerosols and the resulting cloud modifications.

This estimate results in an anthropogenic aerosol effect of about -1.76 ± 0.04 W m^{-2}. Considering only the cloudy-sky fluxes (i.e., the difference between all-sky and clear-sky as diagnosed by EMAC), we obtain a radiative forcing of -1.13 ± 0.03 W m^{-2}. A comparison with the estimates of the IPCC AR5 (Myhre et al., 2013) shows that EMAC-MADE3 lies close

https://doi.org/10.5194/gmd-2019-212
Preprint. Discussion started: 3 September 2019

Geoscientific Model Development Discussions
Open Access
EGU

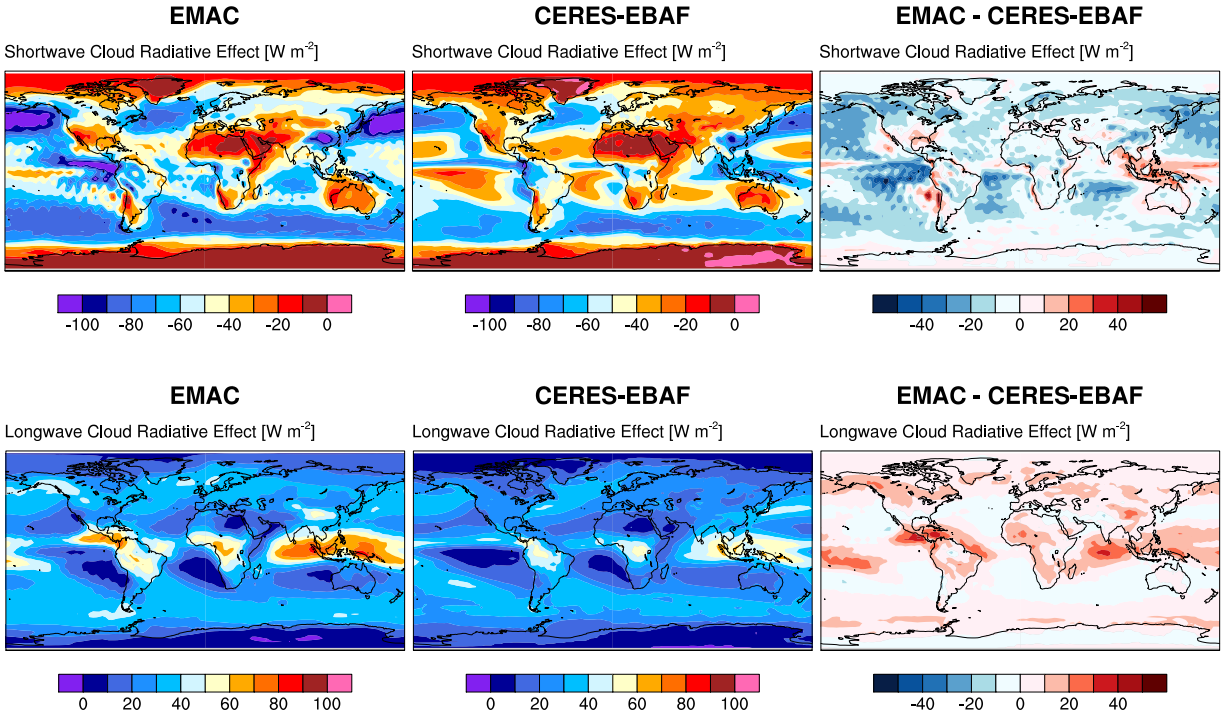

Figure 8. Similar to Fig. 2 but for radiation variables: shortwave (top) and longwave cloud radiative effects (bottom). Satellite data are averaged over the 2003-2015 time period.

to the lower end of the reported range. This implies that EMAC-MADE3 simulates an aerosol effect which is more negative than simulated by most of the participating models: the total aerosol RF reported by the IPCC ranges between -2.05 and 0.05 W m^{-2} (sum of the direct aerosol radiative effect and the indirect effect due to aerosol-induced cloud modifications), with a central value of -0.90 W m^{-2}, while the effect due to aerosol-cloud interactions amounts to -0.45 W m^{-2}, with an uncertainty range from -1.20 and 0 W m^{-2}.

This result shows that EMAC-MADE3 tends to simulate a comparatively high aerosol-induced cooling and could therefore be more sensitive to changes in aerosol concentrations than most of the CMIP5 models. This needs to be kept in mind when applying the model to calculate the climate impacts of specific emission sectors, as it is planned.

Another aspect, which will also be covered by upcoming application studies, is the role of cirrus clouds in the estimates of the climate impact of anthropogenic aerosol. As discussed in the introduction, most of the CMIP5 models do not include aerosol interactions with ice clouds as EMAC-MADE3 is now able to do, which could also explain the larger sensitivity of our model to aerosol perturbations.

https://doi.org/10.5194/gmd-2019-212
Preprint. Discussion started: 3 September 2019

Geoscientific Model Development Discussions

6 Conclusions

In this paper, a new version of the EMAC-MADE3 global aerosol model coupled with a new microphysical cloud scheme has been presented and evaluated. The new cloud scheme features a detailed parameterization for aerosol-driven ice formation within cirrus clouds. The new configuration has been tuned by acting on three cloud microphysical parameters (rate of rain formation by autoconversion, of snow formation by aggregation, and the minimum allowed cloud droplet number concentration) and one aerosol parameter (the size of newly formed aerosol particles by the nucleation process). The optimal values for these four parameters have been chosen by comparing simulated global values of key cloud and radiation variables against several satellite measurements. An in-depth evaluation of the same variables has been performed using a comprehensive set of observations from satellite retrievals and in situ measurements, including data from aircraft-based field campaigns.

The main conclusions on the performance of the coupled version of EMAC-MADE3 can be summarized as follows:

1. EMAC-MADE3 is able to reproduce the global pattern of the main cloud and radiation variables in comparison with satellite data;

2. specific deviations, in particular in the representation of liquid water path, precipitation and cloud radiative effects, mostly confirm known biases of the ECHAM5 model and can therefore not be attributed to the new cloud scheme introduced in this work;

3. a more detailed evaluation of cloud variables in the cirrus regime against an aircraft-based climatology of in situ measurements demonstrates the ability of EMAC-MADE3 to adequately represent ice water content and ice crystal number concentration in cirrus clouds over a wide range of temperatures, albeit with a positive bias for the ice crystal number at higher temperatures;

4. the overall performance of EMAC-MADE3 in simulating global cloud and radiation variables is in line with other coupled models (CMIP5);

5. model biases in the representation of cirrus clouds are common to other models using different parameterizations for aerosol-induced ice formation in cirrus clouds;

6. with regard to the major aerosol features, differences between the coupled model version described here and the uncoupled one are negligible. Hence, the conclusions on the evaluation of aerosol parameters drawn in K19 still hold for the coupled model.

As a first application of the new model system, the anthropogenic aerosol radiative forcing has been calculated and found to be within the range of the estimates from the CMIP5 model ensemble contributing to the IPCC AR5, demonstrating the capabilities of the model to simulate aerosol-induced impacts on the climate system. More targeted applications will include the simulation of the impact of specific emission sectors, such as aviation, on aerosol and clouds, with a specific focus on cirrus clouds, and will be the subject of follow-up studies.

https://doi.org/10.5194/gmd-2019-212
Preprint. Discussion started: 3 September 2019

7 Code availability

MESSy is continuously developed and applied by a consortium of institutions. The usage of MESSy, including MADE3, and access to the source code is licensed to all affiliates of institutions which are members of the MESSy Consortium. Institutions can become members of the MESSy Consortium by signing the MESSy Memorandum of Understanding. More information can be found on the MESSy Consortium Website (http://www.messy-interface.org). The model configuration discussed in this paper has been developed based on version 2.54 and will be part of the next EMAC release (version 2.55).

The Earth System Model eValuation Tool (ESMValTool) v1.1.0, used to produce Figures 2, 4, 7, and 8 is available at https://github.com/ESMValGroup/ESMValTool/releases/tag/v1.1.0.

8 Data availability

The model simulation data analyzed in this work are available upon request and will be published via doi together with the final version of this manuscript.

https://doi.org/10.5194/gmd-2019-212
Preprint. Discussion started: 3 September 2019

Geoscientific Model Development Discussions
Open Access
EGU

Appendix A: Calculation of the number concentration of potential ice-nucleating particles

As mentioned in Sect. 3, MADE3 provides a more detailed description of the aerosol mixing states than HAM, since it is able to distinguish between purely soluble and mixed particles. Therefore, calculating the number of potential INPs as input for the mixed-phase and cirrus cloud parameterizations requires a different approach than in the original K14 cloud scheme. This is outlined here.

We follow the same notation as in K19 and indicate the MADE3 modes Aitken, accumulation and coarse with the index k, a and c, respectively. Mixing states are indicated by s, i and m for soluble, insoluble and mixed, respectively. The number concentration of INPs available for contact freezing in the mixed-phase and for deposition nucleation in the cirrus regime are indicated by $N^{\mathrm{cnt(mp)}}$ and $N^{\mathrm{dep(c)}}$, respectively. Deposition nucleation in mixed-phase clouds is neglected, since observations show that this process is probably not important for ice formation in mixed-phase clouds (Ansmann et al., 2008). In K14, the number of particles available for immersion freezing in mixed-phase clouds was estimated as a fraction of the number of aerosol particles activated to form cloud droplets N^{act}. However, this approach is not suitable for cirrus, where immersion freezing occurs in mixed solution droplets, i.e. aerosol particles that underwent hygroscopic growth, rather than in cloud droplets. A different approach for calculating the number concentration of INPs available for immersion freezing in mixed-phase ($N^{\mathrm{imm(mp)}}$) and cirrus clouds ($N^{\mathrm{imm(c)}}$) is therefore introduced as part of this study. All the number concentrations calculated in this section are checked for consistency in the code, to make sure that the estimated number concentrations in each mode are not larger that the total number concentration in the mode itself. To simplify the notation, this check is not included in the equations below.

We first estimate the number concentration of dust particles in each mode, starting from dust mass concentration and using the conversion function

$$C_{\mathrm{DU}}(D_i,\sigma_i) = \frac{6}{\pi}\frac{1}{D_i^3 \exp(4.5 \ln^2 \sigma_i)\rho}, \tag{A1}$$

with ρ = 2500 kg/m^3 for dust. D_i and σ_i are the lognormal size distribution parameters of mode i, for which we follow the AeroCom recommendations (Dentener et al., 2006): $D_a = 0.42$ μm and $\sigma_a = 1.59$, for the accumulation mode, and $D_c = 1.30$ μm and $\sigma_c = 2.00$, for the coarse mode. The same parameters are also used to calculate the number of emitted dust particles in the model (see Sect. 2). This means that we are neglecting the aging of the size distribution due to dust-dust coagulation. This process has a limited efficiency due to the comparatively small number concentration of mineral dust particles (no dust is present in the Aitken mode given the typically large sizes of mineral dust particles). The number of BC particles is then estimated based on the total number of particles and the number of dust particles as described below.

Since no dust is present in the mixed and insoluble Aitken modes, each particle of these modes contains BC. Note that organic carbon cannot generate BC-free particles in these modes since it is assumed to be emitted internally mixed with BC in the form of "soot" (Kaiser et al., 2019). Furthermore, only the mixed mode BC particles can be activated to form cloud droplets. For mixed-phase clouds, we therefore assume:

$$N_{\mathrm{BC,k}}^{\mathrm{imm(mp)}} = N_{\mathrm{km}}^{\mathrm{act}} \tag{A2}$$

https://doi.org/10.5194/gmd-2019-212
Preprint. Discussion started: 3 September 2019

Geoscientific Model Development Discussions

We do not include contact freezing of BC in the mixed-phase regime as its effect is considered uncertain (Lohmann and Hoose, 2009). For the cirrus regime, the number of potential Aitken-mode-sized INPs which could lead to immersion or deposition freezing coincides with the total number of particles in the mixed or insoluble Aitken mode, respectively:

$$N_{\mathrm{BC,k}}^{\mathrm{imm(c)}} = N_{\mathrm{km}} \qquad N_{\mathrm{BC,k}}^{\mathrm{dep(c)}} = N_{\mathrm{ki}} \tag{A3}$$

In the mixed and insoluble accumulation modes, dust is present in the typical accumulation mode size (see above), since smaller dust particles are not considered and coarse dust particles can only reside in the coarse modes. In this case we estimate the number of dust particles from their mass M using Eq. (A1) and derive the number of potential dust INPs as follows:

$$N_{\mathrm{DU,a}}^{\mathrm{imm(mp)}} = M_{\mathrm{DU,am}}\, C_{\mathrm{DU,a}} \frac{N_{\mathrm{am}}^{\mathrm{act}}}{N_{\mathrm{am}}} \tag{A4}$$

$$N_{\mathrm{DU,a}}^{\mathrm{imm(c)}} = M_{\mathrm{DU,am}}\, C_{\mathrm{DU,a}} \tag{A5}$$

$$N_{\mathrm{DU,a}}^{\mathrm{cnt(mp)}} = M_{\mathrm{DU,ai}}\, C_{\mathrm{DU,a}} \qquad N_{\mathrm{DU,a}}^{\mathrm{dep(c)}} = M_{\mathrm{DU,ai}}\, C_{\mathrm{DU,a}} \tag{A6}$$

It cannot be excluded that these potential dust INPs also contain BC as a consequence of coagulation. Due to the large size of the dust particles compared to BC, we assume however that dust dominates the ice nucleation properties of the particles. The remaining number of particles in the insoluble and mixed accumulation modes can then be ascribed to soot particles (internally mixed black and organic carbon):

$$N_{\mathrm{BC,a}}^{\mathrm{imm(mp)}} = \max(0, N_{\mathrm{am}}^{\mathrm{act}} - N_{\mathrm{DU,a}}^{\mathrm{imm(mp)}}) \tag{A7}$$

$$N_{\mathrm{BC,a}}^{\mathrm{imm(c)}} = \max(0, N_{\mathrm{am}} - N_{\mathrm{DU,a}}^{\mathrm{imm(c)}}) \tag{A8}$$

$$N_{\mathrm{BC,a}}^{\mathrm{dep(c)}} = \max(0, N_{\mathrm{ai}} - N_{\mathrm{DU,a}}^{\mathrm{dep}}) \tag{A9}$$

The insoluble coarse mode is dominated by dust, since it is unlikely that self-coagulation of insoluble accumulation mode BC particles leads to growth into the insoluble coarse mode (BC mass is limited and the self-coagulation frequency is comparatively low). Hence, coarse dust particles are needed to form this mode. This results in:

$$N_{\mathrm{DU,c}}^{\mathrm{cnt(mp)}} = N_{\mathrm{ci}} \qquad N_{\mathrm{DU,c}}^{\mathrm{dep(c)}} = N_{\mathrm{ci}} \tag{A10}$$

$$N_{\mathrm{BC,c}}^{\mathrm{dep(c)}} = 0 \tag{A11}$$

https://doi.org/10.5194/gmd-2019-212
Preprint. Discussion started: 3 September 2019

Geoscientific Model Development Discussions

In the mixed coarse mode the mixing state is uncertain, since particles can be composed of dust from both the accumulation and the coarse size range, whose relative contribution is not known. Therefore mass-to-number conversion is not as straightforward as in the accumulation mode case. We need to distinguish two cases, based on the relative abundance of dust particles. We define the dust number fraction in this mode as:

$$f_{\mathrm{DU}} = \frac{M_{\mathrm{DU,cm}}\, C_{\mathrm{DU,c}}}{N_{\mathrm{cm}}} \tag{A12}$$

We use the conversion factor $C_{\mathrm{DU,c}}$ of coarse dust particles to estimate the number fraction, since these particles dominate the dust mass (possible mass contributions of accumulation mode dust are small, according to Dentener et al., 2006). Hence, an estimate of the coarse dust particle number based on the total dust mass in the mode appears to be a good approximation. It provides a minimum estimate of the number of dust containing particles in the mode, since also many accumulation-mode-sized dust particles might be present in the mode due to coagulation. For dust-dominated regimes, e.g. at or in the vicinity of deserts, it can be expected that f_{DU} is large and that also the non-coarse-dust particles in the mode contain many accumulation-mode-sized dust immersions. It can also be expected that BC has a comparatively small contribution under these conditions. Hence, all particles of the mode can be regarded as possible dust ice-nucleating particles. In the present study we assume dust dominance where $f_{\mathrm{DU}} \geq 0.7$. In this case, the above assumptions result in:

$$N_{\mathrm{DU,c}}^{\mathrm{imm(mp)}} = N_{\mathrm{cm}}^{\mathrm{act}} \tag{A13}$$

$$N_{\mathrm{DU,c}}^{\mathrm{imm(c)}} = N_{\mathrm{cm}} \tag{A14}$$

$$N_{\mathrm{BC,c}}^{\mathrm{imm(mp)}} = 0 \qquad N_{\mathrm{BC,c}}^{\mathrm{imm(c)}} = 0 \tag{A15}$$

If $f_{\mathrm{DU}} < 0.7$ we assume that BC plays a major role and that the minimum estimate of the number of dust containing particles applies. This results in:

$$N_{\mathrm{DU,c}}^{\mathrm{imm(mp)}} = M_{\mathrm{DU,cm}}\, C_{\mathrm{DU,c}}\, \frac{N_{\mathrm{cm}}^{\mathrm{act}}}{N_{\mathrm{cm}}} \tag{A16}$$

$$N_{\mathrm{DU,c}}^{\mathrm{imm(c)}} = M_{\mathrm{DU,cm}}\, C_{\mathrm{DU,c}} \tag{A17}$$

$$N_{\mathrm{BC,c}}^{\mathrm{imm(mp)}} = \max(0, N_{\mathrm{cm}}^{\mathrm{act}} - N_{\mathrm{DU,c}}^{\mathrm{imm(mp)}}) \tag{A18}$$

$$N_{\mathrm{BC,c}}^{\mathrm{imm(c)}} = \max(0, N_{\mathrm{cm}} - N_{\mathrm{DU,c}}^{\mathrm{imm(c)}}). \tag{A19}$$

Despite the admittedly many assumptions required to estimate the number of coarse immersion INPs, we note that the resulting uncertainties are probably small, since the contribution of coarse particles to the number concentration of INPs is mostly small

https://doi.org/10.5194/gmd-2019-212
Preprint. Discussion started: 3 September 2019

compared to the corresponding contribution of the accumulation mode. Sensitivity studies show little to no variation in ice water content and ice crystal number concentration for values of f_{DU} ranging from 0.6 to 0.9.

Author contributions. MR conceived the study, implemented the new cloud scheme in EMAC, designed and performed the simulations, analyzed the data, evaluated and interpreted the results, and wrote the paper. JH conceived the study, contributed to the interpretation of the results and to the text. UL provided the new cloud scheme, contributed to design the simulations and to interpret the results; CB, with the help of BH and IT, developed and implemented the method for filtering online dust emissions at low model resolutions in EMAC; MK and CR provided the in situ data for the evaluation of the cirrus properties and contributed to the interpretation of the results; VH, RH and CV provided the DACCIWA and ML-CIRRUS data for the evaluation of cloud droplet number concentrations and of cirrus properties, and contributed to the interpretation of the results and to the text.

Competing interests. The authors declare that they have no conflict of interest.

Acknowledgements. This study was supported by the DLR transport programme (projects *Transport and the Environment - VEU2* and *Transport and Climate - TraK*), by the DLR space research programme (project *Climate relevant trace gases, aerosols and clouds - KliSAW*) by the DLR aviation research programme (project *Eco-efficient air travel - Eco2Fly*) and by the Initiative and Networking Fund of the Helmholtz Association through the project *Advanced Earth System Modelling Capacity (ESM)*. The EMAC simulations were preformed at the German Climate Computing Center (DKRZ, Hamburg, Germany). The ML-CIRRUS campaign was supported by DFG SPP HALO1294 contract no VO1504/4-1, and Romy Heller by the EU ICE-GENESIS project within H2020 grant agreement no. 824310. The contribution of cloud sonde data from ML-CIRRUS by Stephan Borrmann and Ralf Weigel (University of Mainz and MPI-C, Germany) is kindly acknowledged. We are grateful to Yvonne Boose (DLR, Germany) for her comments and suggestions on an earlier version of the manuscript, and to Klaus Gierens, Patrick Jöckel, Bernd Kärcher, Axel Lauer, Matthias Nützel (DLR, Germany), Holger Tost (University of Mainz, Germany), Sara Bacer (MPI-C, Germany) and Miriam Kuebbeler for helpful discussions. The development work presented in this paper has greatly benefited from the support of the whole MESSy team of developers and maintainers.

https://doi.org/10.5194/gmd-2019-212
Preprint. Discussion started: 3 September 2019

References

Abdul-Razzak, H. and Ghan, S. J.: A parameterization of aerosol activation: 2. Multiple aerosol types, J. Geophys. Res. Atmos., 105, 6837–6844, doi:10.1029/1999JD901161, 2000.

Adler, R. F., Huffman, G. J., Chang, A., Ferraro, R., Xie, P.-P., Janowiak, J., Rudolf, B., Schneider, U., Curtis, S., Bolvin, D., Gruber, A., Susskind, J., Arkin, P., and Nelkin, E.: The Version-2 Global Precipitation Climatology Project (GPCP) Monthly Precipitation Analysis (1979-Present), J. Hydrometeorol., 4, 1147–1167, doi:10.1175/1525-7541(2003)004<1147:TVGPCP>2.0.CO;2, 2003.

Afchine, A., Rolf, C., Costa, A., Spelten, N., Riese, M., Buchholz, B., Ebert, V., Heller, R., Kaufmann, S., Minikin, A., Voigt, C., Zöger, M., Smith, J., Lawson, P., Lykov, A., Khaykin, S., and Krämer, M.: Ice particle sampling from aircraft – influence of the probing position on the ice water content, Atmos. Meas. Tech., 11, 4015–4031, doi:10.5194/amt-11-4015-2018, https://www.atmos-meas-tech.net/11/4015/2018/, 2018.

Andreae, M. O., Jones, C. D., and Cox, P. M.: Strong present-day aerosol cooling implies a hot future, Nature, 435, 1187–1190, doi:10.1038nature03671, 2005.

Ansmann, A., Tesche, M., Althausen, D., Müller, D., Seifert, P., Freudenthaler, V., Heese, B., Wiegner, M., Pisani, G., Knippertz, P., and Dubovik, O.: Influence of Saharan dust on cloud glaciation in southern Morocco during the Saharan Mineral Dust Experiment, J. Geophys. Res., 113, doi:10.1029/2007JD008785, 2008.

Bacer, S., Sullivan, S. C., Karydis, V. A., Barahona, D., Krämer, M., Nenes, A., Tost, H., Tsimpidi, A. P., Lelieveld, J., and Pozzer, A.: Implementation of a comprehensive ice crystal formation parameterization for cirrus and mixed-phase clouds in the EMAC model (based on MESSy 2.53), Geosci. Model Dev., 11, 4021–4041, doi:10.5194/gmd-11-4021-2018, 2018.

Barahona, D. and Nenes, A.: Parameterizing the competition between homogeneous and heterogeneous freezing in cirrus cloud formation – monodisperse ice nuclei, Atmos. Chem. Phys., 9, 369–381, doi:10.5194/acp-9-369-2009, 2009.

Bennartz, R.: Global assessment of marine boundary layer cloud droplet number concentration from satellite, J. Geophys. Res. Atmos., 112, doi:10.1029/2006JD007547, 2007.

Bennartz, R. and Rausch, J.: Global and regional estimates of warm cloud droplet number concentration based on 13 years of AQUA-MODIS observations, Atmos. Chem. Phys., 17, 9815–9836, doi:10.5194/acp-17-9815-2017, 2017.

Bergeron, T.: Über die dreidimensional verknüpfende Wetteranalyse, Phd, Norske Videnskabs Akademie, Oslo, 1928.

Boucher, O., Randall, D., Artaxo, P., Bretherton, C., Feingold, G., Forster, P., Kerminen, V.-M., Kondo, Y., Liao, H., Lohmann, U., Rasch, P., Satheesh, S., Sherwood, S., Stevens, B., and Zhang, X.: Clouds and Aerosols, book section 7, pp. 571–658, Cambridge University Press, Cambridge, United Kingdom and New York, NY, USA, doi:10.1017/CBO9781107415324.016, 2013.

Cheng, T., Peng, Y., Feichter, J., and Tegen, I.: An improvement on the dust emission scheme in the global aerosol-climate model ECHAM5-HAM, Atmos. Chem. Phys., 8, 1105–1117, 2008.

Cziczo, D. J., Froyd, K. D., Hoose, C., Jensen, E. J., Diao, M., Zondlo, M. A., Smith, J. B., Twohy, C. H., and Murphy, D. M.: Clarifying the Dominant Sources and Mechanisms of Cirrus Cloud Formation, Science, 340, 1320–1324, doi:10.1126/science.1234145, 2013.

David, R. O., Marcolli, C., Fahrni, J., Qiu, Y., Perez Sirkin, Y. A., Molinero, V., Mahrt, F., Brühwiler, D., Lohmann, U., and Kanji, Z. A.: Pore condensation and freezing is responsible for ice formation below water saturation for porous particles, Proc. Natl. Acad. Sci. Unit. States Am., doi:10.1073/pnas.1813647116, 2019.

https://doi.org/10.5194/gmd-2019-212
Preprint. Discussion started: 3 September 2019

de Reus, M., Borrmann, S., Bansemer, A., Heymsfield, A. J., Weigel, R., Schiller, C., Mitev, V., Frey, W., Kunkel, D., Kürten, A., Curtius, J., Sitnikov, N. M., Ulanovsky, A., and Ravegnani, F.: Evidence for ice particles in the tropical stratosphere from in-situ measurements, Atmos. Chem. Phys., 9, 6775–6792, doi:10.5194/acp-9-6775-2009, 2009.

Dentener, F., Kinne, S., Bond, T., Boucher, O., Cofala, J., Generoso, S., Ginoux, P., Gong, S., Hoelzemann, J. J., Ito, A., Marelli, L., Penner, J. E., Putaud, J.-P., Textor, C., Schulz, M., van der Werf, G. R., and Wilson, J.: Emissions of primary aerosol and precursor gases in the years 2000 and 1750 prescribed data-sets for AeroCom, Atmos. Chem. Phys., 6, 4321–4344, doi:10.5194/acp-6-4321-2006, 2006.

Dietmüller, S., Jöckel, P., Tost, H., Kunze, M., Gellhorn, C., Brinkop, S., Frömming, C., Ponater, M., Steil, B., Lauer, A., and Hendricks, J.: A new radiation infrastructure for the Modular Earth Submodel System (MESSy, based on version 2.51), Geosci. Model Dev., 9, 2209–2222, doi:10.5194/gmd-9-2209-2016, 2016.

Elsaesser, G. S., O'Dell, C. W., Lebsock, M. D., Bennartz, R., Greenwald, T. J., and Wentz, F. J.: The Multisensor Advanced Climatology of Liquid Water Path (MAC-LWP), J. Clim., 30, 10 193–10 210, doi:10.1175/JCLI-D-16-0902.1, 2017.

Eyring, V., Righi, M., Lauer, A., Evaldsson, M., Wenzel, S., Jones, C., Anav, A., Andrews, O., Cionni, I., Davin, E. L., Deser, C., Ehbrecht, C., Friedlingstein, P., Gleckler, P., Gottschaldt, K.-D., Hagemann, S., Juckes, M., Kindermann, S., Krasting, J., Kunert, D., Levine, R., Loew, A., Mäkelä, J., Martin, G., Mason, E., Phillips, A. S., Read, S., Rio, C., Roehrig, R., Senftleben, D., Sterl, A., van Ulft, L. H., Walton, J., Wang, S., and Williams, K. D.: ESMValTool (v1.0) – a community diagnostic and performance metrics tool for routine evaluation of Earth system models in CMIP, Geosci. Model Dev., 9, 1747–1802, doi:10.5194/gmd-9-1747-2016, 2016.

Findeisen, W.: Kolloid-meteorologische Vorgänge bei Niederschlagsbildung, Meteorol. Z., 55, 121–133, 1938.

Flamant, C., Knippertz, P., Fink, A. H., Akpo, A., Brooks, B., Chiu, C. J., Coe, H., Danuor, S., Evans, M., Jegede, O., Kalthoff, N., Konaré, A., Liousse, C., Lohou, F., Mari, C., Schlager, H., Schwarzenboeck, A., Adler, B., Amekudzi, L., Aryee, J., Ayoola, M., Batenburg, A. M., Bessardon, G., Borrmann, S., Brito, J., Bower, K., Burnet, F., Catoire, V., Colomb, A., Denjean, C., Fosu-Amankwah, K., Hill, P. G., Lee, J., Lothon, M., Maranan, M., Marsham, J., Meynadier, R., Ngamini, J.-B., Rosenberg, P., Sauer, D., Smith, V., Stratmann, G., Taylor, J. W., Voigt, C., and Yoboué, V.: The Dynamics-Aerosol-Chemistry-Cloud Interactions in West Africa Field Campaign: Overview and Research Highlights, B. Am. Meteorol. Soc., 99, 83–104, doi:10.1175/BAMS-D-16-0256.1, 2018.

Gettelman, A. and Chen, C.: The climate impact of aviation aerosols, Geophys. Res. Lett., 40, 2785–2789, doi:10.1002/grl.50520, 2013.

Gettelman, A., Liu, X., Ghan, S. J., Morrison, H., Park, S., Conley, A. J., Klein, S. A., Boyle, J., Mitchell, D. L., and Li, J.-L. F.: Global simulations of ice nucleation and ice supersaturation with an improved cloud scheme in the Community Atmosphere Model, J. Geophys. Res. Atmos., 115, doi:10.1029/2009JD013797, 2010.

Ghan, S. J., Abdul-Razzak, H., Nenes, A., Ming, Y., Liu, X., Ovchinnikov, M., Shipway, B., Meskhidze, N., Xu, J., and Shi, X.: Droplet nucleation: Physically-based parameterizations and comparative evaluation, J. Adv. Model. Earth Syst., 3, n/a–n/a, doi:10.1029/2011MS000074, m10001, 2011.

Gläser, G., Kerkweg, A., and Wernli, H.: The Mineral Dust Cycle in EMAC 2.40: sensitivity to the spectral resolution and the dust emission scheme, Atmos. Chem. Phys., 12, 1611–1627, doi:10.5194/acp-12-1611-2012, 2012.

Guelle, W., Schulz, M., Balkanski, Y., and Dentener, F.: Influence of the source formulation on modeling the atmospheric global distribution of sea salt aerosol, J. Geophys. Res. Atmos., 106, 27 509–27 524, doi:10.1029/2001JD900249, 2001.

Hendricks, J., Kärcher, B., and Lohmann, U.: Effects of ice nuclei on cirrus clouds in a global climate model, J. Geophys. Res. Atmos., 116, n/a–n/a, doi:10.1029/2010JD015302, d18206, 2011.

Hoose, C. and Möhler, O.: Heterogeneous ice nucleation on atmospheric aerosols: a review of results from laboratory experiments, Atmos. Chem. Phys., 12, 9817–9854, doi:10.5194/acp-12-9817-2012, 2012.

https://doi.org/10.5194/gmd-2019-212
Preprint. Discussion started: 3 September 2019

Geoscientific Model Development Discussions

Hoose, C., Lohmann, U., Erdin, R., and Tegen, I.: The global influence of dust mineralogical composition on heterogeneous ice nucleation in mixed-phase clouds, Environ. Res. Lett., 3, 025 003, doi:10.1088/1748-9326/3/2/025003, 2008.

Huneeus, N., Schulz, M., Balkanski, Y., Griesfeller, J., Prospero, J., Kinne, S., Bauer, S., Boucher, O., Chin, M., Dentener, F., Diehl, T., Easter, R., Fillmore, D., Ghan, S., Ginoux, P., Grini, A., Horowitz, L., Koch, D., Krol, M. C., Landing, W., Liu, X., Mahowald, N., Miller, R., Morcrette, J.-J., Myhre, G., Penner, J., Perlwitz, J., Stier, P., Takemura, T., and Zender, C. S.: Global dust model intercomparison in AeroCom phase I, Atmos. Chem. Phys., 11, 7781–7816, doi:10.5194/acp-11-7781-2011, 2011.

Jöckel, P., Kerkweg, A., Pozzer, A., Sander, R., Tost, H., Riede, H., Baumgaertner, A., Gromov, S., and Kern, B.: Development cycle 2 of the Modular Earth Submodel System (MESSy2), Geosci. Model Dev., 3, 717–752, doi:10.5194/gmd-3-717-2010, 2010.

Joos, H., Spichtinger, P., Lohmann, U., Gayet, J.-F., and Minikin, A.: Orographic cirrus in the global climate model ECHAM5, J. Geophys. Res. Atmos., 113, doi:10.1029/2007JD009605, 2008.

Kaiser, J. C., Hendricks, J., Righi, M., Riemer, N., Zaveri, R. A., Metzger, S., and Aquila, V.: The MESSy aerosol submodel MADE3 (v2.0b): description and a box model test, Geosci. Model Dev., 7, 1137–1157, doi:10.5194/gmd-7-1137-2014, 2014.

Kaiser, J. C., Hendricks, J., Righi, M., Jöckel, P., Tost, H., Kandler, K., Weinzierl, B., Sauer, D., Heimerl, K., Schwarz, J. P., Perring, A. E., and Popp, T.: Global aerosol modeling with MADE3 (v3.0) in EMAC (based on v2.53): model description and evaluation, Geosci. Model Dev., 12, 541–579, doi:10.5194/gmd-12-541-2019, 2019.

Kanji, Z. A., Ladino, L. A., Wex, H., Boose, Y., Burkert-Kohn, M., Cziczo, D. J., and Krämer, M.: Overview of Ice Nucleating Particles, Meteorological Monographs, 58, 1.1–1.33, doi:10.1175/AMSMONOGRAPHS-D-16-0006.1, 2017.

Kärcher, B. and Lohmann, U.: A parameterization of cirrus cloud formation: Homogeneous freezing of supercooled aerosols, J. Geophys. Res. Atmos., 107, AAC 4–1–AAC 4–10, doi:10.1029/2001JD000470, 2002.

Kärcher, B., Hendricks, J., and Lohmann, U.: Physically based parameterization of cirrus cloud formation for use in global atmospheric models, J. Geophys. Res. Atmos., 111, n/a–n/a, doi:10.1029/2005JD006219, d01205, 2006.

Karydis, V. A., Kumar, P., Barahona, D., Sokolik, I. N., and Nenes, A.: On the effect of dust particles on global cloud condensation nuclei and cloud droplet number, J. Geophys. Res. Atmos., 116, n/a–n/a, doi:10.1029/2011JD016283, d23204, 2011.

Karydis, V. A., Tsimpidi, A. P., Bacer, S., Pozzer, A., Nenes, A., and Lelieveld, J.: Global impact of mineral dust on cloud droplet number concentration, Atmos. Chem. Phys., 17, 5601–5621, doi:10.5194/acp-17-5601-2017, 2017.

Kaufmann, S., Voigt, C., Jurkat, T., Thornberry, T., Fahey, D. W., Gao, R.-S., Schlage, R., Schäuble, D., and Zöger, M.: The airborne mass spectrometer AIMS – Part 1: AIMS-H_2O for UTLS water vapor measurements, Atmos. Meas. Techn., 9, 939–953, doi:10.5194/amt-9-939-2016, https://www.atmos-meas-tech.net/9/939/2016/, 2016.

Kaufmann, S., Voigt, C., Heller, R., Jurkat-Witschas, T., Krämer, M., Rolf, C., Zöger, M., Giez, A., Buchholz, B., Ebert, V., Thornberry, T., and Schumann, U.: Intercomparison of midlatitude tropospheric and lower-stratospheric water vapor measurements and comparison to ECMWF humidity data, Atmos. Chem. Phys., 18, 16 729–16 745, doi:10.5194/acp-18-16729-2018, 2018.

Kleine, J., Voigt, C., Sauer, D., Schlager, H., Scheibe, M., Jurkat-Witschas, T., Kaufmann, S., Kärcher, B., and Anderson, B. E.: In Situ Observations of Ice Particle Losses in a Young Persistent Contrail, Geophys. Res. Lett., 45, 13 553–13 561, doi:10.1029/2018GL079390, 2018.

Koehler, K. A., DeMott, P. J., Kreidenweis, S. M., Popovicheva, O. B., Petters, M. D., Carrico, C. M., Kireeva, E. D., Khokhlova, T. D., and Shonija, N. K.: Cloud condensation nuclei and ice nucleation activity of hydrophobic and hydrophilic soot particles, Phys. Chem. Chem. Phys., 11, 7906–7920, doi:10.1039/B905334B, 2009.

https://doi.org/10.5194/gmd-2019-212
Preprint. Discussion started: 3 September 2019

Koop, T., Luo, B., Tsias, A., and Peter, T.: Water activity as the determinant for homogeneous ice nucleation in aqueous solutions, Nature, 406, 611–614, doi:10.1038/35020537, 2000.

Krämer, M., Schiller, C., Afchine, A., Bauer, R., Gensch, I., Mangold, A., Schlicht, S., Spelten, N., Sitnikov, N., Borrmann, S., de Reus, M., and Spichtinger, P.: Ice supersaturations and cirrus cloud crystal numbers, Atmos. Chem. Phys., 9, 3505–3522, doi:10.5194/acp-9-3505-2009, 2009.

Krämer, M., Rolf, C., Luebke, A., Afchine, A., Spelten, N., Costa, A., Meyer, J., Zöger, M., Smith, J., Herman, R. L., Buchholz, B., Ebert, V., Baumgardner, D., Borrmann, S., Klingebiel, M., and Avallone, L.: A microphysics guide to cirrus clouds – Part 1: Cirrus types, Atmos. Chem. Phys., 16, 3463–3483, doi:10.5194/acp-16-3463-2016, 2016.

Kuebbeler, M., Lohmann, U., Hendricks, J., and Kärcher, B.: Dust ice nuclei effects on cirrus clouds, Atmos. Chem. Phys., 14, 3027–3046, doi:10.5194/acp-14-3027-2014, 2014.

Kulkarni, G., China, S., Liu, S., Nandasiri, M., Sharma, N., Wilson, J., Aiken, A. C., Chand, D., Laskin, A., Mazzoleni, C., Pekour, M., Shilling, J., Shutthanandan, V., Zelenyuk, A., and Zaveri, R. A.: Ice nucleation activity of diesel soot particles at cirrus relevant temperature conditions: Effects of hydration, secondary organics coating, soot morphology, and coagulation, Geophys. Res. Lett., 43, 3580–3588, doi:10.1002/2016GL068707, 2016GL068707, 2016.

Lamarque, J.-F., Bond, T. C., Eyring, V., Granier, C., Heil, A., Klimont, Z., Lee, D., Liousse, C., Mieville, A., Owen, B., Schultz, M. G., Shindell, D., Smith, S. J., Stehfest, E., Van Aardenne, J., Cooper, O. R., Kainuma, M., Mahowald, N., McConnell, J. R., Naik, V., Riahi, K., and van Vuuren, D. P.: Historical (1850-2000) gridded anthropogenic and biomass burning emissions of reactive gases and aerosols: methodology and application, Atmos. Chem. Phys., 10, 7017–7039, doi:10.5194/acp-10-7017-2010, 2010.

Lamarque, J.-F., Shindell, D. T., Josse, B., Young, P. J., Cionni, I., Eyring, V., Bergmann, D., Cameron-Smith, P., Collins, W. J., Doherty, R., Dalsoren, S., Faluvegi, G., Folberth, G., Ghan, S. J., Horowitz, L. W., Lee, Y. H., MacKenzie, I. A., Nagashima, T., Naik, V., Plummer, D., Righi, M., Rumbold, S. T., Schulz, M., Skeie, R. B., Stevenson, D. S., Strode, S., Sudo, K., Szopa, S., Voulgarakis, A., and Zeng, G.: The Atmospheric Chemistry and Climate Model Intercomparison Project (ACCMIP): overview and description of models, simulations and climate diagnostics, Geosci. Model Dev., 6, 179–206, doi:10.5194/gmd-6-179-2013, 2013.

Lauer, A. and Hamilton, K.: Simulating Clouds with Global Climate Models: A Comparison of CMIP5 Results with CMIP3 and Satellite Data, J. Clim., 26, 3823–3845, doi:10.1175/JCLI-D-12-00451.1, 2013.

Lauer, A., Eyring, V., Righi, M., Buchwitz, M., Defourny, P., Evaldsson, M., Friedlingstein, P., de Jeu, R., de Leeuw, G., Loew, A., Merchant, C. J., Müller, B., Popp, T., Reuter, M., Sandven, S., Senftleben, D., Stengel, M., Roozendael, M. V., Wenzel, S., and Willèn, U.: Benchmarking CMIP5 models with a subset of ESA CCI Phase 2 data using the ESMValTool, Rem. Sens. Environ., 203, 9 – 39, doi:https://doi.org/10.1016/j.rse.2017.01.007, 2017.

Lohmann, U. and Diehl, K.: Sensitivity Studies of the Importance of Dust Ice Nuclei for the Indirect Aerosol Effect on Stratiform Mixed-Phase Clouds, J. Atmos. Sci., 63, 968–982, doi:10.1175/JAS3662.1, 2006.

Lohmann, U. and Ferrachat, S.: Impact of parametric uncertainties on the present-day climate and on the anthropogenic aerosol effect, Atmos. Chem. Phys., 10, 11 373–11 383, doi:10.5194/acp-10-11373-2010, 2010.

Lohmann, U. and Hoose, C.: Sensitivity studies of different aerosol indirect effects in mixed-phase clouds, Atmos. Chem. Phys., 9, 8917–8934, doi:10.5194/acp-9-8917-2009, 2009.

Lohmann, U. and Kärcher, B.: First interactive simulations of cirrus clouds formed by homogeneous freezing in the ECHAM general circulation model, J. Geophys. Res. Atmos., 107, doi:10.1029/2001JD000767, 2002.

https://doi.org/10.5194/gmd-2019-212
Preprint. Discussion started: 3 September 2019

Lohmann, U. and Neubauer, D.: The importance of mixed-phase and ice clouds for climate sensitivity in the global aerosol–climate model ECHAM6-HAM2, Atmos. Chem. Phys., 18, 8807–8828, doi:10.5194/acp-18-8807-2018, 2018.

Lohmann, U., Stier, P., Hoose, C., Ferrachat, S., Kloster, S., Roeckner, E., and Zhang, J.: Cloud microphysics and aerosol indirect effects in the global climate model ECHAM5-HAM, Atmos. Chem. Phys., 7, 3425–3446, doi:10.5194/acp-7-3425-2007, 2007.

Lohmann, U., Spichtinger, P., Jess, S., Peter, T., and Smit, H.: Cirrus cloud formation and ice supersaturated regions in a global climate model, Environ. Res. Lett., 3, 045 022, doi:10.1088/1748-9326/3/4/045022, 2008.

Mahrt, F., Marcolli, C., David, R. O., Grönquist, P., Barthazy Meier, E. J., Lohmann, U., and Kanji, Z. A.: Ice nucleation abilities of soot particles determined with the Horizontal Ice Nucleation Chamber, Atmos. Chem. Phys., 18, 13 363–13 392, doi:10.5194/acp-18-13363-2018, 2018.

Marcolli, C.: Pre-activation of aerosol particles by ice preserved in pores, Atmos. Chem. Phys., 17, 1595–1622, doi:10.5194/acp-17-1595-2017, 2017.

McFiggans, G., Artaxo, P., Baltensperger, U., Coe, H., Facchini, M. C., Feingold, G., Fuzzi, S., Gysel, M., Laaksonen, A., Lohmann, U., Mentel, T. F., Murphy, D. M., O'Dowd, C. D., Snider, J. R., and Weingartner, E.: The effect of physical and chemical aerosol properties on warm cloud droplet activation, Atmos. Chem. Phys., 6, 2593–2649, doi:10.5194/acp-6-2593-2006, 2006.

Möhler, O., Field, P. R., Connolly, P., Benz, S., Saathoff, H., Schnaiter, M., Wagner, R., Cotton, R., Krämer, M., Mangold, A., and Heymsfield, A. J.: Efficiency of the deposition mode ice nucleation on mineral dust particles, Atmos. Chem. Phys., 6, 3007–3021, doi:10.5194/acp-6-3007-2006, 2006.

Möhler, O., Benz, S., Saathoff, H., Schnaiter, M., Wagner, R., Schneider, J., Walter, S., Ebert, V., and Wagner, S.: The effect of organic coating on the heterogeneous ice nucleation efficiency of mineral dust aerosols, Environ. Res. Lett., 3, 025 007, doi:10.1088/1748-9326/3/2/025007, 2008.

Murphy, D. M. and Koop, T.: Review of the vapour pressures of ice and supercooled water for atmospheric applications, Q J Roy. Meteorol. Soc., 131, 1539–1565, doi:10.1256/qj.04.94, 2005.

Myhre, G., Shindell, D., Breéon, F.-M., Collins, W., Fuglestvedt, J., Huang, J., Koch, D., Lamarque, J.-F., Lee, D., Mendoza, B., Nakajima, T., Robock, A., Stephens, G., Takemura, T., and Zhang, H.: Anthropogenic and Natural Radiative Forcing, book section 8, pp. 659–740, Cambridge University Press, Cambridge, United Kingdom and New York, NY, USA, doi:10.1017/CBO9781107415324.018, 2013.

Penner, J. E., Quaas, J., Storelvmo, T., Takemura, T., Boucher, O., Guo, H., Kirkevåg, A., Kristjánsson, J. E., and Seland, Ø.: Model intercomparison of indirect aerosol effects, Atmos. Chem. Phys., 6, 3391–3405, doi:10.5194/acp-6-3391-2006, 2006.

Penner, J. E., Zhou, C., Garnier, A., and Mitchell, D. L.: Anthropogenic Aerosol Indirect Effects in Cirrus Clouds, J. Geophys. Res. Atmos., 123, 11,652–11,677, doi:10.1029/2018JD029204, 2018.

Petters, M. D. and Kreidenweis, S. M.: A single parameter representation of hygroscopic growth and cloud condensation nucleus activity, Atmos. Chem. Phys., 7, 1961–1971, doi:10.5194/acp-7-1961-2007, 2007.

Pringle, K. J., Tost, H., Pozzer, A., Pöschl, U., and Lelieveld, J.: Global distribution of the effective aerosol hygroscopicity parameter for CCN activation, Atmos. Chem. Phys., 10, 5241–5255, doi:10.5194/acp-10-5241-2010, 2010.

Räisänen, P. and Järvinen, H.: Impact of cloud and radiation scheme modifications on climate simulated by the ECHAM5 atmospheric GCM, Q J Roy. Meteorol. Soc., 136, 1733–1752, doi:10.1002/qj.674, 2010.

Righi, M., Hendricks, J., and Sausen, R.: The global impact of the transport sectors on atmospheric aerosol: simulations for year 2000 emissions, Atmos. Chem. Phys., 13, 9939–9970, doi:10.5194/acp-13-9939-2013, 2013.

https://doi.org/10.5194/gmd-2019-212
Preprint. Discussion started: 3 September 2019

Righi, M., Eyring, V., Gottschaldt, K.-D., Klinger, C., Frank, F., Jöckel, P., and Cionni, I.: Quantitative evaluation of ozone and selected climate parameters in a set of EMAC simulations, Geosci. Model Dev., 8, 733–768, doi:10.5194/gmd-8-733-2015, 2015a.

Righi, M., Hendricks, J., and Sausen, R.: The global impact of the transport sectors on atmospheric aerosol in 2030 – Part 1: Land transport and shipping, Atmos. Chem. Phys., 15, 633–651, doi:10.5194/acp-15-633-2015, 2015b.

Righi, M., Hendricks, J., and Sausen, R.: The global impact of the transport sectors on atmospheric aerosol in 2030 – Part 2: Aviation, Atmos. Chem. Phys., 16, 4481–4495, doi:10.5194/acp-16-4481-2016, 2016.

Roeckner, E., Brokopf, R., Esch, M., Giorgetta, M., Hagemann, S., Kornblueh, L., Manzini, E., Schlese, U., and Schulzweida, U.: Sensitivity of Simulated Climate to Horizontal and Vertical Resolution in the ECHAM5 Atmosphere Model, J. Clim., 19, 3771–3791, doi:10.1175/JCLI3824.1, 2006.

Rothenberg, D., Avramov, A., and Wang, C.: On the representation of aerosol activation and its influence on model-derived estimates of the aerosol indirect effect, Atmos. Chem. Phys., 18, 7961–7983, doi:10.5194/acp-18-7961-2018, 2018.

Spichtinger, P. and Gierens, K. M.: Modelling of cirrus clouds – Part 1a: Model description and validation, Atmos. Chem. Phys., 9, 685–706, doi:10.5194/acp-9-685-2009, 2009.

Stengel, M., Stapelberg, S., Sus, O., Schlundt, C., Poulsen, C., Thomas, G., Christensen, M., Carbajal Henken, C., Preusker, R., Fischer, J., Devasthale, A., Willén, U., Karlsson, K.-G., McGarragh, G. R., Proud, S., Povey, A. C., Grainger, R. G., Meirink, J. F., Feofilov, A., Bennartz, R., Bojanowski, J. S., and Hollmann, R.: Cloud property datasets retrieved from AVHRR, MODIS, AATSR and MERIS in the framework of the Cloud_cci project, Earth System Science Data, 9, 881–904, doi:10.5194/essd-9-881-2017, 2017.

Stier, P., Feichter, J., Kinne, S., Kloster, S., Vignati, E., Wilson, J., Ganzeveld, L., Tegen, I., Werner, M., Balkanski, Y., Schulz, M., Boucher, O., Minikin, A., and Petzold, A.: The aerosol-climate model ECHAM5-HAM, Atmos. Chem. Phys., 5, 1125–1156, doi:10.5194/acp-5-1125-2005, 2005.

Sundqvist, H., Berge, E., and Kristjánsson, J. E.: Condensation and Cloud Parameterization Studies with a Mesoscale Numerical Weather Prediction Model, Monthly Weather Review, 117, 1641–1657, doi:10.1175/1520-0493(1989)117<1641:CACPSW>2.0.CO;2, 1989.

Taylor, J. W., Haslett, S. L., Bower, K., Flynn, M., Crawford, I., Dorsey, J., Choularton, T., Connolly, P. J., Hahn, V., Voigt, C., Sauer, D., Dupuy, R., Brito, J., Schwarzenboeck, A., Bourriane, T., Denjean, C., Rosenberg, P., Flamant, C., Lee, J. D., Vaughan, A. R., Hill, P. G., Brooks, B., Catoire, V., Knippertz, P., and Coe, H.: Aerosol influences on low-level clouds in the West African monsoon, Atmospheric Chemistry and Physics Discussions, 2019, 1–45, doi:10.5194/acp-2019-40, 2019.

Tegen, I., Harrison, S. P., Kohfeld, K., Prentice, I. C., Coe, M., and Heimann, M.: Impact of vegetation and preferential source areas on global dust aerosol: Results from a model study, J. Geophys. Res. Atmos., 107, 14–1–14–27, doi:10.1029/2001JD000963, 2002.

Tegen, I., Werner, M., Harrison, S., and Kohfeld, K.: Relative importance of climate and land use in determining present and future global soil dust emission, Geophys. Res. Lett., 31, L05 105, doi:10.1029/2003GL019216, 2004.

Urbanek, B., Groß, S., Wirth, M., Rolf, C., Krämer, M., and Voigt, C.: High Depolarization Ratios of Naturally Occurring Cirrus Clouds Near Air Traffic Regions Over Europe, Geophys. Res. Lett., 45, 13 166–13 172, doi:10.1029/2018GL079345, 2018.

Vali, G., DeMott, P. J., Möhler, O., and Whale, T. F.: Technical Note: A proposal for ice nucleation terminology, Atmos. Chem. Phys., 15, 10 263–10 270, doi:10.5194/acp-15-10263-2015, 2015.

Voigt, C., Jessberger, P., Jurkat, T., Kaufmann, S., Baumann, R., Schlager, H., Bobrowski, N., Giuffrida, G., and Salerno, G.: Evolution of CO_2, SO_2, HCl, and HNO_3 in the volcanic plumes from Etna, Geophys. Res. Lett., 41, 2196–2203, doi:10.1002/2013GL058974, 2014.

https://doi.org/10.5194/gmd-2019-212
Preprint. Discussion started: 3 September 2019

Voigt, C., Schumann, U., Minikin, A., Abdelmonem, A., Afchine, A., Borrmann, S., Boettcher, M., Buchholz, B., Bugliaro, L., Costa, A., Curtius, J., Dollner, M., Dörnbrack, A., Dreiling, V., Ebert, V., Ehrlich, A., Fix, A., Forster, L., Frank, F., Fütterer, D., Giez, A., Graf, K., Grooß, J.-U., Groß, S., Heimerl, K., Heinold, B., Hüneke, T., Järvinen, E., Jurkat, T., Kaufmann, S., Kenntner, M., Klingebiel, M., Klimach, T., Kohl, R., Krämer, M., Krisna, T. C., Luebke, A., Mayer, B., Mertes, S., Molleker, S., Petzold, A., Pfeilsticker, K., Port, M., Rapp, M., Reutter, P., Rolf, C., Rose, D., Sauer, D., Schäfler, A., Schlage, R., Schnaiter, M., Schneider, J., Spelten, N., Spichtinger, P., Stock, P., Walser, A., Weigel, R., Weinzierl, B., Wendisch, M., Werner, F., Wernli, H., Wirth, M., Zahn, A., Ziereis, H., and Zöger, M.: ML-CIRRUS: The Airborne Experiment on Natural Cirrus and Contrail Cirrus with the High-Altitude Long-Range Research Aircraft HALO, B. Am. Meteorol. Soc., 98, 271–288, doi:10.1175/BAMS-D-15-00213.1, 2017.

Waliser, D. E., Li, J.-L. F., Woods, C. P., Austin, R. T., Bacmeister, J., Chern, J., Del Genio, A., Jiang, J. H., Kuang, Z., Meng, H., Minnis, P., Platnick, S., Rossow, W. B., Stephens, G. L., Sun-Mack, S., Tao, W.-K., Tompkins, A. M., Vane, D. G., Walker, C., and Wu, D.: Cloud ice: A climate model challenge with signs and expectations of progress, J. Geophys. Res. Atmos., 114, n/a–n/a, doi:10.1029/2008JD010015, d00A21, 2009.

Weigel, R., Spichtinger, P., Mahnke, C., Klingebiel, M., Afchine, A., Petzold, A., Krämer, M., Costa, A., Molleker, S., Reutter, P., Szakáll, M., Port, M., Grulich, L., Jurkat, T., Minikin, A., and Borrmann, S.: Thermodynamic correction of particle concentrations measured by underwing probes on fast-flying aircraft, Atmos. Meas. Tech., 9, 5135–5162, doi:10.5194/amt-9-5135-2016, 2016.

Zhou, C. and Penner, J. E.: Aircraft soot indirect effect on large-scale cirrus clouds: Is the indirect forcing by aircraft soot positive or negative?, J. Geophys. Res. Atmos., 119, 11,303–11,320, doi:10.1002/2014JD021914, 2014JD021914, 2014.